Carranza-Torres, C. (2023). Scaled power law failure criteria for intact rock and rockfill shear interfaces and their application to problems of borehole damage and slope stability. Keynote Lecture. In *Proceedings of Primer Congreso Chileno de Mecanica de Rocas 2023 (First Chilean Rock Mechanics Congress)*. Santiago. Chile. November 22–24, 2023.

A video presentation of this article can be accessed by clicking the link below:

Link to video presentation.

Primer Congreso Chileno | Mecanica de Rocas 2023
Suzuki K., Jarufe J., Silva M. & Villouta A. (Eds)

Scaled power law failure criteria for intact rock and rockfill shear interfaces and their application to problems of borehole damage and slope stability

C. Carranza-Torres

Department of Civil Engineering, University of Minnesota, Duluth Campus, Minnesota, USA

ABSTRACT

This paper presents the formulation of a general power law failure criterion expressed in terms of principal stresses, and normal and shear stresses on the failure plane. The Mohr-Coulomb and Hoek-Brown failure criteria are shown to be particular cases of the general power law failure criterion. The Griffith failure criterion for intact rock, and the generalization of this criterion proposed by Fairhurst in 1964, are also shown to be particular cases of the general power law failure criterion. A scaling rule for the mathematical expressions conforming the power law failure criterion is presented, and its application in the interpretation of triaxial tests results in samples of intact rock that obey the Hoek-Brown and Fairhurst criteria is discussed. A power law failure criterion for uncemented rockfill originally proposed by de Mello, and later generalized by Indraratna et al. in 1993, are also shown to be particular cases of the general power law failure criterion proposed in this paper. Scaling of these failure criteria for rockfill shear interfaces is discussed and illustrated with the analysis of triaxial test results of large rockfill samples. The paper addresses then the problem of assessing damage around boreholes in intact rock by estimation of extent of plastic failure and wall convergence of the borehole. Application of the scaled form of the Mohr-Coulomb, Hoek-Brown and Fairhurst failure criteria is shown to lead to compact dimensionless representations of the extent of plastic failure and borehole wall convergence. Finally the paper addresses the problem of determining the factor of safety of slopes made of uncemented rockfill, showing again how the scaled form of the general power law failure criterion leads to compact dimensionless representations of the slope stability solution. By providing transformation equations and benchmark problems, this paper also intends to contribute to the needed implementation of new material constitutive models in finite element and finite difference software used in practical geomechanics, in particular a power law failure criterion for modelling cemented and uncemented rockfill.

KEYWORDS

Failure criterion; power law; borehole damage; rockfill slope

1. INTRODUCTION

One of the first failure criteria proposed for intact rock is the Griffith criterion —Griffith (1921; 1924); Murrell (1958). The Griffith failure criterion is based on the assumption that the combination of principal stresses defining failure of the rock is such that the maximum tensile stress at the tip of an open crack oriented in the least favorable direction will reach some limiting critical value. After reaching this critical value, the crack will begin to propagate, leading to failure of the rock.

When expressed in terms of major and minor principal stresses, σ_1 and σ_3, respectively, the Griffith failure criterion is a power law function of the form (see, for example, Jaeger, Cook, & Zimmerman 2007)

$$\frac{\sigma_1}{\sigma_c} = \frac{\sigma_3}{\sigma_c} + \sqrt{2\frac{\sigma_3}{\sigma_c} + \frac{1}{4}} + \frac{1}{2} \qquad \text{if} \qquad \frac{\sigma_1}{\sigma_c} \geq \frac{3}{8} \tag{1}$$

and a linear function of the form

$$\frac{\sigma_3}{\sigma_c} = -\frac{1}{8} \qquad \text{if} \qquad \frac{\sigma_1}{\sigma_c} \leq \frac{3}{8} \tag{2}$$

In equations (1) and (2), σ_c is the unconfined compressive strength of the rock (a positive quantity, since in the equations above and in all equations that follow, compression will be assumed positive).

Also, when expressed in terms of shear and normal stresses on the failure plane, τ_s and σ_n, respectively, the Griffith failure criterion is a power law function of the form

$$\frac{\tau_s}{\sigma_c} = \frac{1}{2}\sqrt{2\frac{\sigma_n}{\sigma_c} + \frac{1}{4}} \tag{3}$$

The tensile strength of the rock, σ_t (a negative quantity according to the assumed sign convention), can be obtained by making $\sigma_1 = 0$ and $\sigma_3 = \sigma_t$ in equation (1), or $\tau_s = 0$ and $\sigma_n = \sigma_t$ in equation (3). This gives

$$-\frac{\sigma_t}{\sigma_c} = \frac{1}{8} \tag{4}$$

Therefore, according to the Griffith failure criterion, the absolute value of the ratio of unconfined compressive strength and tensile strength of the rock is equal to 8.

Experimental testing of intact rock samples shows that the ratio $-\sigma_t/\sigma_c$ is not necessarily equal to 8 and it can be lower or more typically larger than the value 8 predicted by the Griffith failure criterion. Different failure criteria have been proposed to account for this variability of the ratio $-\sigma_t/\sigma_c$. A popular failure criterion is the Hoek-Brown failure criterion (Hoek & Brown 1980a; 1980b) which was derived based on triaxial, unconfined compression, and tensile strength test results for intact rock samples, taking as a basis the Griffith failure criterion and the linear Mohr-Coulomb failure criterion. Another failure criterion is the so called Fairhurst criterion (Fairhurst 1964, Hoek & Martin 2014). This criterion is basically the generalization of the Griffith criterion in which the ratio $-\sigma_t/\sigma_c$ is a variable.

As it will be shown in this paper, all mentioned failure criteria have two main features: 1) they can all be written in terms of two material parameters, these being the unconfined compressive strength of the rock, σ_c, and the ratio of tensile and compression strength; $-\sigma_t/\sigma_c$; 2) they can all be written as power law functions, involving principal stresses or stresses on the failure plane.

Power law functions are also used to predict the shear strength of rockfill interfaces. For example, for the case of uncemented rockfill, de Mello (1977) proposed the following failure criterion in terms of shear and normal stresses on the failure plane, τ_s and σ_n, respectively,

$$\tau_s = a\,\sigma_n^b \tag{5}$$

In equation (5), a and b are constants.

Also for uncemented rockfill interfaces, Indraratna, Wijewardena, & Balasubramaniam (1993) proposed a similar expression as equation (5), but scaling the stresses with a representative average of the unconfined

compressive strength of the rock fragments, σ_{cF}, i.e.,

$$\frac{\tau_s}{\sigma_{cF}} = A\left(\frac{\sigma_n}{\sigma_{cF}}\right)^B \tag{6}$$

In equation (6), A and B are constants, that can be related to the constants in equation (5) using the following relationships

$$A = \frac{a}{\sigma_{cF}^{1-B}} \quad \text{and} \quad B = b \tag{7}$$

Although the use of numerical modelling tools based on finite element or finite difference methods has become a standard practice in rock engineering design, it is somehow surprising that these numerical tools do not implement constitutive models for rockfill according to the power law models by de Mello or Indraratna et al.; the explanation may be related to the difficultly of expressing the mentioned failure criteria in terms of principal stresses. With this in mind, this paper presents the equations needed to recast the failure criteria by de Mello and Indraratna et al. in terms of principal stresses.

Considering the relevance that power law material models have in the prediction of the shear strength of intact rock and rockfill interfaces, the main objective of this paper is to present a general power law failure criterion for intact rock and rockfill interfaces that has the failure criteria mentioned above —i.e., the Griffith, Hoek-Brown, Mohr-Coulomb and Fairhurst failure criteria for intact rock, and the de Mello and Indraratna et al. for uncemented rockfill— as particular forms of the general criterion. In doing so, the paper will introduce a rule for scaling the proposed general power law failure criterion, and as a result, for scaling the mentioned failure criteria. The advantages of using the scaled form of power law failure criteria will be illustrated with two rock engineering examples, namely, the analysis of damage in boreholes in intact rock that obeys the Mohr-Coulomb, Hoek-Brown and Fairhurst failure criterion; and the analysis of stability of rockfill embankments, when the rockfill obeys the Indraratna et al. failure criterion.

2. POWER LAW FAILURE CRITERIA FOR INTACT ROCK

2.1. General form of the power law failure criterion

The first form of the general power law failure criterion applies to intact rock, and involves the major and minor principal stresses, σ_1 and σ_3, respectively. The failure criterion is as follows

$$\frac{\sigma_1}{\sigma_c} = \frac{\sigma_3}{\sigma_c} + C\left(\frac{\sigma_3}{\sigma_c} - \frac{\sigma_{tBx}}{\sigma_c}\right)^D + E \tag{8}$$

In equation (8), C, D and E are constants, σ_c is the unconfined compressive strength and σ_{tBx} is the so called biaxial tensile strength of the intact rock.

The failure criterion is schematically represented in Figure 1a. Noticing that the axes represent principal stresses divided by σ_c, point U_c corresponds to the unconfined (or uniaxial) compressive strength of the rock, σ_c, and point B_t corresponds to the biaxial tensile strength of the rock, σ_{tBx}.

Because the ordinate of point U_c in Figure 1a must be one, the following relationship between the parameters in equation (8) must hold

$$C\left(-\frac{\sigma_{tBx}}{\sigma_c}\right)^D + E = 1 \tag{9}$$

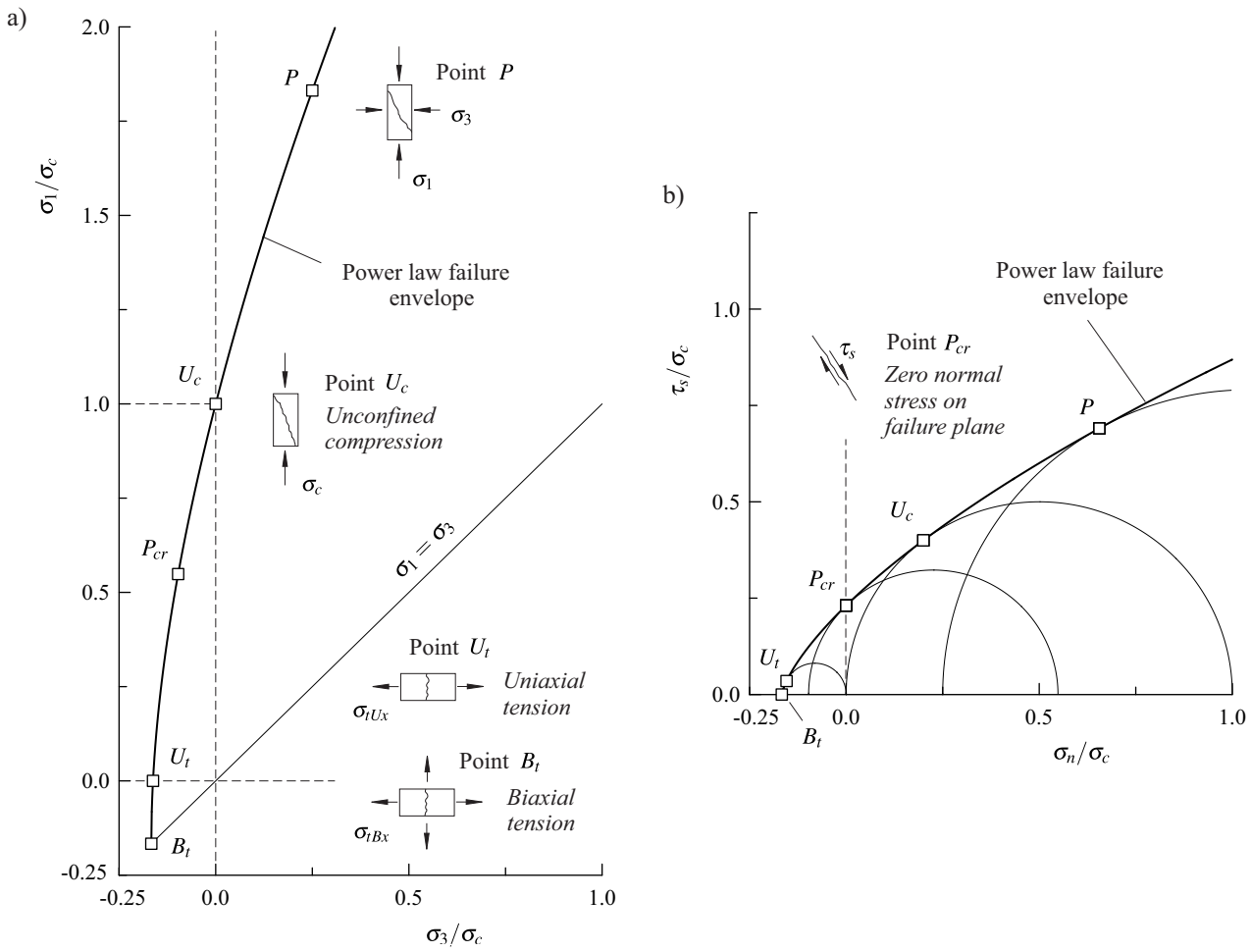

Figure 1. General power law failure criterion expressed in terms of a) minor and major principal stresses and b) normal and shear stresses on the failure plane.

The failure criterion given by equation (8) can be recast as an equivalent failure criterion expressed in terms of shear and normal stresses on the failure plane by a set of parametric equations of the form

$$\frac{\sigma_n}{\sigma_c} = f_{\sigma n}\left(\frac{\sigma_1}{\sigma_c}, \frac{\sigma_3}{\sigma_c}, \frac{\sigma_{tBx}}{\sigma_c}, C, D, E\right) \tag{10}$$

$$\frac{\tau_s}{\sigma_c} = f_{\tau s}\left(\frac{\sigma_1}{\sigma_c}, \frac{\sigma_3}{\sigma_c}, \frac{\sigma_{tBx}}{\sigma_c}, C, D, E\right) \tag{11}$$

The explicit form of the equations above are presented in Appendix A.

Figure 1b represents the same failure criterion given by equation (8), expressed now in terms of shear and normal stresses on the failure plane (divided by σ_c), after application of equations (10) and (11). Mohr-circles constructed based on the principal stresses had been added to the diagram, so the points of tangency of the circles with the failure envelope in Figure 1b define the same points indicated in Figure 1a.

Besides the points B_t and U_t discussed earlier on, other points representing particular stress states are indicated in Figure 1a. For example, point P corresponds to the general case of confined compression. Point P_{cr}, coordinates of which can be obtained from equations (10) and (11) by making $\sigma_n = 0$, corresponds the case of zero normal stress acting on the failure plane (it can be argued that this stress state is a limiting case

for which the Mohr failure model loses validity, as friction requires the normal stress on the frictional surface to be compressive —see, for example, Jaeger et al. 2007). Point U_t corresponds to the uniaxial tensile stress state, associated with the uniaxial tensile strength, σ_{tUx} —which can be obtained from equation (8), considering that $\sigma_{tUx} = \sigma_3$ when $\sigma_1 = 0$.

Two observations must be made regarding the failure criteria representations in Figure 1. The first is with regard to the points B_t and U_t, representing the biaxial tensile strength, σ_{tBx}, and the uniaxial tensile strength, σ_{tUx}, respectively. From a mechanical point of view, there is no reason to expect σ_{tBx} to be different from σ_{tUx} (i.e., points B_t and U_t not to be aligned vertically). The fact that they are different, as indicated in Figure 1, is that a tension cut-off needs to be introduced for the failure criterion. This will become evident later on, when the different failure criteria introduced in Section 1 are analyzed in more depth.

The second observation is with regard to the constant D in equation (8). The maximum value for this constant is one, otherwise the failure envelope in Figure 1a will be concave upwards, and therefore will not conform to a fundamental postulate of the theory of plasticity —Davis & Selvadurai (2002). The minimum value of the constant D is such that once the failure criterion given by equation (8) is recast in terms of stresses on the failure plane (i.e., with equations 10 and 11) the curvature of the resulting failure envelope allows the Mohr circle construction at every point of the envelope, with a the circle touching the envelope at the point of tangency only.

The second form of the general power law failure criterion for intact rock, adapted version of which will be applied to rockfill interfaces later on, involves the shear and normal stresses on the failure plane, τ_s and σ_n, respectively. The failure criterion is as follows

$$\frac{\tau_s}{\sigma_c} = A\left(\frac{\sigma_n}{\sigma_c} - \frac{\sigma_{tBx}}{\sigma_c}\right)^B \tag{12}$$

In equation (12), A and B are constants, σ_c is the unconfined compressive strength and σ_{tBx} is the biaxial tensile strength.

The maximum value for the constant B in equation (12) is one, for the same reason stated for the constant D above. The minimum value is 0.5, because otherwise the failure envelope does not allow a Mohr circle construction —i.e., the construction of a circle that is tangent to the curve, and that touches the curve at the point of tangency only (see Jiang et al. 2003, Baker 2004).

The failure criterion given by equation (12) can be recast as an equivalent failure criterion expressed in terms of principal stresses by a set of parametric equations of the form

$$\frac{\sigma_3}{\sigma_c} = f_{\sigma 3}\left(\frac{\tau_s}{\sigma_c}, \frac{\sigma_n}{\sigma_c}, \frac{\sigma_{tBx}}{\sigma_c}, A, B\right) \tag{13}$$

$$\frac{\sigma_1}{\sigma_c} = f_{\sigma 1}\left(\frac{\tau_s}{\sigma_c}, \frac{\sigma_n}{\sigma_c}, \frac{\sigma_{tBx}}{\sigma_c}, A, B\right) \tag{14}$$

Equations (13) and (14), which are basically the inverse of equations (10) and (11), can be combined into a single equation that defines the failure criterion in terms of principal stresses σ_1 and σ_3. The equation is provided in Appendix A.

In the following sections, the Mohr-Coulomb, Hoek-Brown and Fairhurst failure criteria are discussed in more depth, and are shown to be particular cases of the general power law failure criteria given by equations (8) and (12).

2.2. The Mohr-Coulomb failure criterion

The Mohr-Coulomb failure criterion expressed in terms of principal stresses σ_1 and σ_3 can be written as follows (see for example, Goodman 1989; Davis & Selvadurai 2002)

$$\frac{\sigma_1}{\sigma_c} = \frac{1+\sin\phi}{1-\sin\phi}\,\frac{\sigma_3}{\sigma_c} + 1 \tag{15}$$

where

$$\sigma_c = 2c\sqrt{\frac{1+\sin\phi}{1-\sin\phi}} \tag{16}$$

In equations (15) and (16), ϕ is the internal friction angle and c is the cohesion.

The ratio of unconfined compression strength and biaxial tensile strength, to be designated as r_i, is written as follows,

$$r_i = -\frac{\sigma_c}{\sigma_{tBx}} \tag{17}$$

The relationship between the ratio r_i and ϕ can be obtained by making $\sigma_1 = \sigma_3 = \sigma_{tBx}$ in equation (15), which together with equation (17) gives

$$r_i = \frac{2\sin\phi}{1-\sin\phi} \qquad \text{or} \qquad \phi = \arcsin\left(\frac{r_i}{r_i+2}\right) \tag{18}$$

Combining equation (17) and the first equation (18), and replacing into equation (15), the Mohr-Coulomb failure criterion expressed in terms of principal stresses can also be written as follows

$$\frac{\sigma_1}{\sigma_c} = (r_i+1)\,\frac{\sigma_3}{\sigma_c} + 1 \qquad \text{or} \qquad \frac{\sigma_1}{\sigma_c} = \frac{\sigma_3}{\sigma_c} + r_i\left(\frac{\sigma_3}{\sigma_c} - \frac{\sigma_{tBx}}{\sigma_c}\right) \tag{19}$$

Comparing the second equation (19) with equation (8), the Mohr-Coulomb failure criterion is found to be a particular case of the general power law failure criterion given by equation (8) when

$$C = r_i \qquad D = 1 \quad \text{and} \quad E = 0 \tag{20}$$

It should be noticed that the constants C, D and E given by equation (20), satisfy the equation (9).

The Mohr-Coulomb failure criterion given by equations (19) is represented graphically Figure 2a. The diagram includes failure envelopes corresponding to different values of the ratio r_i. As a reference, the Griffith failure envelope that according to equation (4) corresponds to a ratio of compressive-to-tensile strength equal to 8, is also represented in Figure 2a. Considering that the Griffith failure criterion and the Mohr-Coulomb failure criterion corresponding to $r_i = 8$ are equivalent (in that the mentioned ratio is the same), it is noticeable from Figure 2a that the strength predicted by the Mohr-Coulomb failure criterion in the compressive confining stress regime is significantly larger than the one predicted by the Griffith failure criterion —and the opposite is true in the tensile confining stress regime.

Figure 2a includes failure envelopes for two limiting cases of the ratio r_i, namely $r_i = 0$ and $r_i = \infty$.

For the first case, the resulting failure criterion is obtained by making $r_i = 0$ in the first of equations (19),

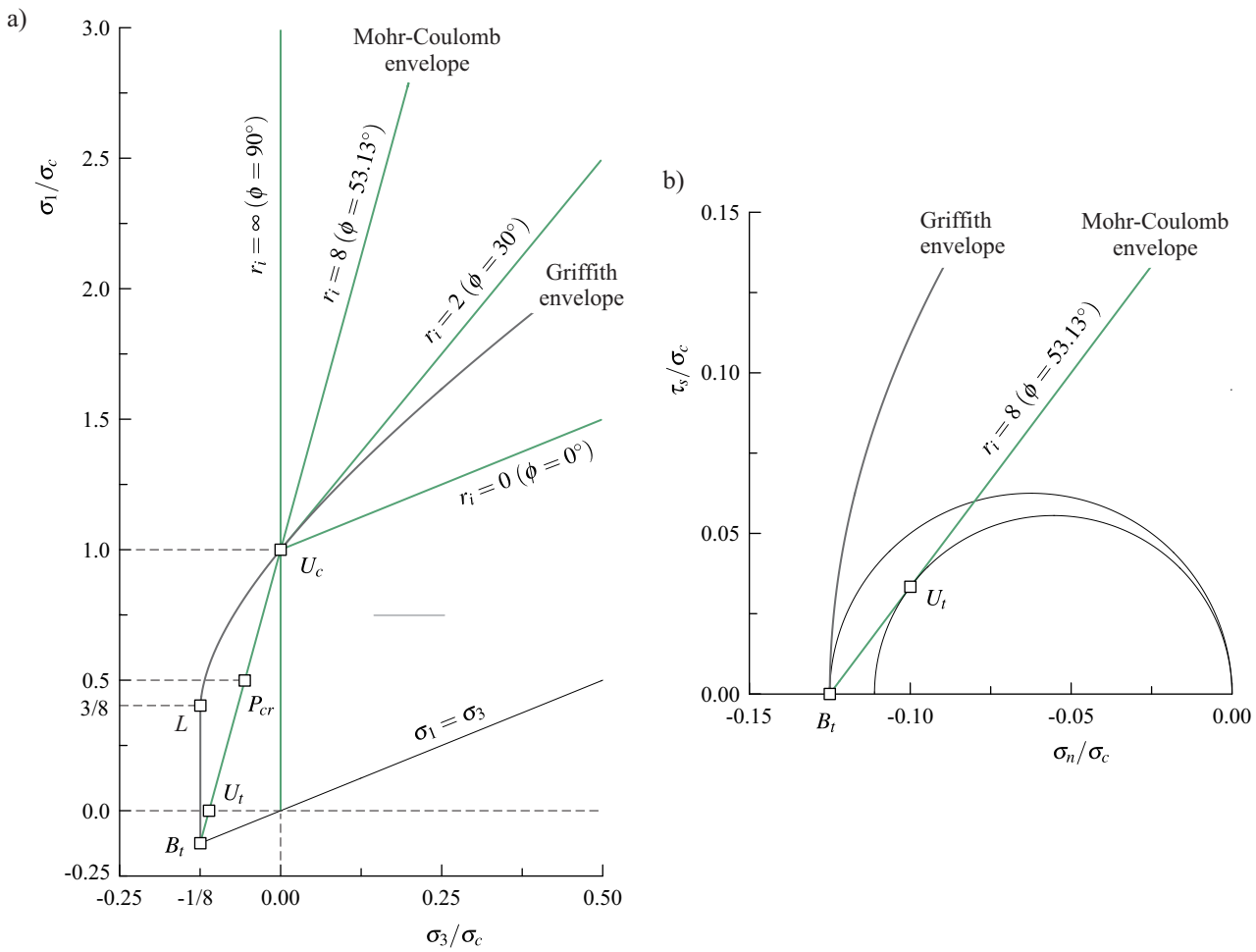

Figure 2. Mohr-Coulomb failure criterion for different compression-to-tension strength ratios, r_i, expressed in terms of a) principal stresses and b) stresses on the failure plane. The Griffith failure criterion is included for comparison.

i.e.,

$$\frac{\sigma_1}{\sigma_c} = \frac{\sigma_3}{\sigma_c} + 1 \tag{21}$$

which corresponds to the failure criterion of a frictionless (cohesive only) material —and therefore to a failure envelope parallel to the bisector line $\sigma_1 = \sigma_3$ in Figure 2a.

For the second case, the resulting failure criterion is obtained by taking the limit when r_i tends to ∞ in the first of equations (19), i.e.,

$$\frac{\sigma_1}{\sigma_c} \to \infty \tag{22}$$

which means that when the ratio of biaxial tensile strength and compressive strength is zero, the predicted major principal stress at failure is unbounded —and the failure envelope becomes a vertical line, as represented in Figure 2a.

Figure 2a shows the points B_t and U_t (see also Figure 1a) for the failure envelope corresponding to $r_i = 8$. According to the first observation made in Section 2.1, for the Mohr-Coulomb failure criterion these points do not align vertically, and the uniaxial tensile strength (σ_{tUx}) associated with point U_t is smaller, in absolute value, than the biaxial tensile strength (σ_{tBx}) associated with point B_t. Indeed, making $\sigma_3 = \sigma_{tUx}$ and $\sigma_1 = 0$

in the first of equations (19), the uniaxial tensile strength (divided by σ_c) is

$$\frac{\sigma_{tUx}}{\sigma_c} = -\frac{1}{r_i + 1} \tag{23}$$

Considering that σ_{tBx} is related to the ratio r_i according to equation (17), the ratio of uniaxial-to-biaxial tensile strength results to be

$$\frac{\sigma_{tUx}}{\sigma_{tBx}} = \frac{r_i}{r_i + 1} < 1 \tag{24}$$

Since the uniaxial tensile strength (or a mesure of this strength) can be obtained by indirect Brazilian splitting tests or direct tensile strength tests, the Mohr-Coulomb failure criterion requires a tension cut-off at point U_t or at a point to the right side of point U_t in Figure 2a —see, for example, Goodman (1989).

The Mohr-Coulomb failure criterion expressed in terms of normal and shear stresses (divided by the unconfined compressive strength) is written as follows (see for example, Goodman 1989; Davis & Selvadurai 2002)

$$\frac{\tau_s}{\sigma_c} = \tan\phi \, \frac{\sigma_n}{\sigma_c} + \frac{c}{\sigma_c} \tag{25}$$

Application of equations (10) and (11) to the first of equations (19), allows the Mohr-Coulomb failure criterion to be written in terms of the ratio r_i as follows

$$\frac{\tau_s}{\sigma_c} = \frac{r_i}{2\sqrt{r_i + 1}} \, \frac{\sigma_n}{\sigma_c} + \frac{1}{2\sqrt{r_i + 1}} \tag{26}$$

It should be noticed that by making $\tau_s = 0$ and $\sigma_n = \sigma_{tBx}$ in equation (26), the following expression is obtained

$$\frac{\sigma_{tBx}}{\sigma_c} = -\frac{1}{r_i} \tag{27}$$

which is basically the same equation (17).

The Mohr-Coulomb failure criterion given by equations (26) for the particular case $r_i = 8$ and for negative values of σ_n/σ_c is represented graphically Figure 2b. The Griffith failure criterion is included as a reference. As mentioned earlier on, the strength predicted by the Griffith failure criterion is larger than the one predicted by the Mohr-Coulomb failure criterion in the tensile confining stress regime.

Combining equations (26) and (27), the Mohr-Coulomb failure criterion expressed in terms of normal and shear stresses on the failure place can be written as follows

$$\frac{\tau_s}{\sigma_c} = \frac{r_i}{2\sqrt{r_i + 1}} \left(\frac{\sigma_n}{\sigma_c} - \frac{\sigma_{tBx}}{\sigma_c} \right) \tag{28}$$

Comparing equation (28) with equation (12), the constants A and B in equation (12) result to be

$$A = \frac{r_i}{2\sqrt{r_i + 1}} \quad \text{and} \quad B = 1 \tag{29}$$

In view of equations (19) and (28), the Mohr-Coulomb failure criterion is therefore shown to be a particular case of the general power law failure criteria expressed in terms of principal stresses (equation 8) and in terms of stresses on the failure plane (equation 12), respectively.

2.3. The Hoek-Brown failure criterion

The origin of the Hoek-Brown failure criterion for intact rock can be traced back to the diagram in Figure 3 (Hoek 1965; Hoek & Bieniawski 1966). In this diagram the dots represent results of triaxial, unconfined compression and tensile strength tests for a large variety of rock types compiled by Hoek (the dots identified as Set 2, 10, 11, 15 and 17 are highlighted in the diagram, as these will be discussed in a later section in this paper). The figure includes the Griffith failure envelope, and Mohr-Coulomb failure envelopes corresponding to different values of friction coefficients, μ. The Mohr-Coulomb failure criterion was interpreted to be a *modified* version of the Griffith failure criterion, when the crack, in the Griffith model, has been assumed to be closed and to be frictional.

Figure 3 shows that the major principal stress at failure predicted by the Griffith model is significantly lower than measured from tests; it also shows that the major principal stress at failure predicted by the Mohr-Coulomb model, with expected values of friction angle for the crack wall, is higher than measured from tests, particularly as the confining stress increases. All this probably led Hoek and Brown to propose a failure criterion with a similar form as the Griffith criterion (i.e., with a square root affecting the minor principal stress), that predicted higher values of major principal stress at failure than the Griffith failure criterion, and that adjusted better to the test results.

The Hoek-Brown failure criterion for intact rock was first published in Hoek & Brown (1980a; 1980b) . Expressed in terms of principal stresses, σ_1 and σ_3, the failure criterion is written as follows

$$\frac{\sigma_1}{\sigma_c} = \frac{\sigma_3}{\sigma_c} + \sqrt{m_i \frac{\sigma_3}{\sigma_c} + 1} \tag{30}$$

where σ_c is the unconfined compression strength of the intact rock and m_i is a rock parameter.

Considering that the biaxial tensile strength, σ_{tBx}, corresponds to the case, $\sigma_1 = \sigma_3$ in equation (30), then

$$m_i = -\frac{\sigma_c}{\sigma_{tBx}} \qquad \text{or} \qquad \frac{\sigma_{tBx}}{\sigma_c} = -\frac{1}{m_i} \tag{31}$$

Replacing the second equation (31) into equation (30), and factoring terms, the Hoek-Brown failure criterion can be written as follows

$$\frac{\sigma_1}{\sigma_c} = \frac{\sigma_3}{\sigma_c} + \sqrt{m_i}\sqrt{\frac{\sigma_3}{\sigma_c} - \frac{\sigma_{tBx}}{\sigma_c}} \tag{32}$$

Comparing equation (32) with equation (8), the Hoek-Brown failure criterion is found to be a particular case of the general power law failure criterion given by equation (8) when

$$C = \sqrt{m_i} \qquad D = \frac{1}{2} \quad \text{and} \quad E = 0 \tag{33}$$

with these constants also satisfying the equation (9).

The Hoek-Brown failure criterion given by equations (30) is represented graphically in Figure 4a. The diagram includes different failure envelopes corresponding to different values of the parameter m_i. As a reference, the Griffith failure envelope and the Mohr-Coulomb failure envelope for $r_i = 8$ are also represented in Figure 4a. Considering that the Hoek-Brown failure envelope for $m_i = 8$ is comparable to the mentioned Griffith and Mohr-Coulomb envelopes (in that the compressive-to-tensile strength ratio is the same), Figure 4a shows that the Hoek-Brown failure envelope is an *intermediate* failure envelope that lies in between the

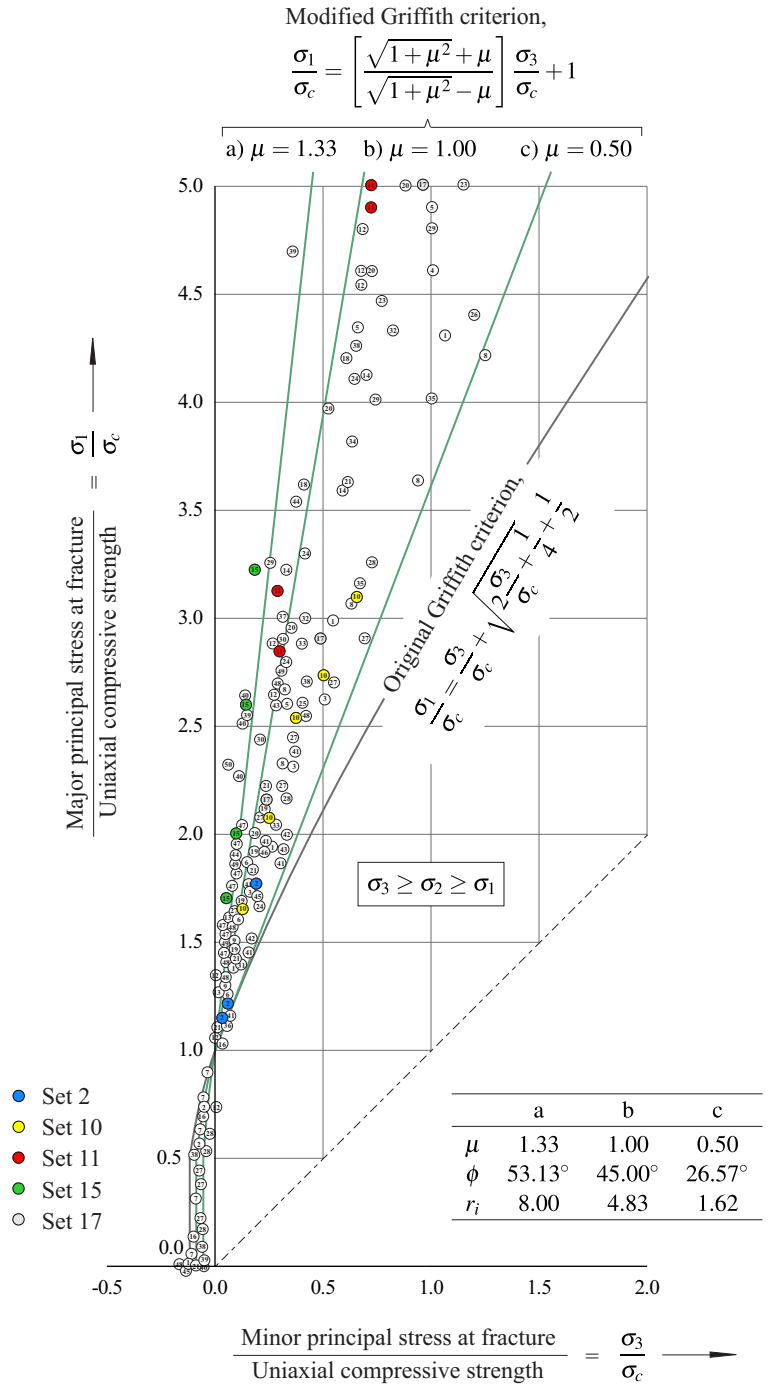

Figure 3. Triaxial test results on samples of various rock types compiled by Hoek (1965) —see also Hoek & Bieniawski (1966). The table at the bottom includes the relationship between represented values of friction coefficient, μ, and the ratio r_i given by equation (18).

mentioned Griffith and Mohr-Coulomb failure envelopes, in both, compression and tension confining stress regimes.

Figure 4a also includes failure envelopes for two limiting cases of the ratio m_i, namely $m_i = 0$ and $m_i = \infty$.

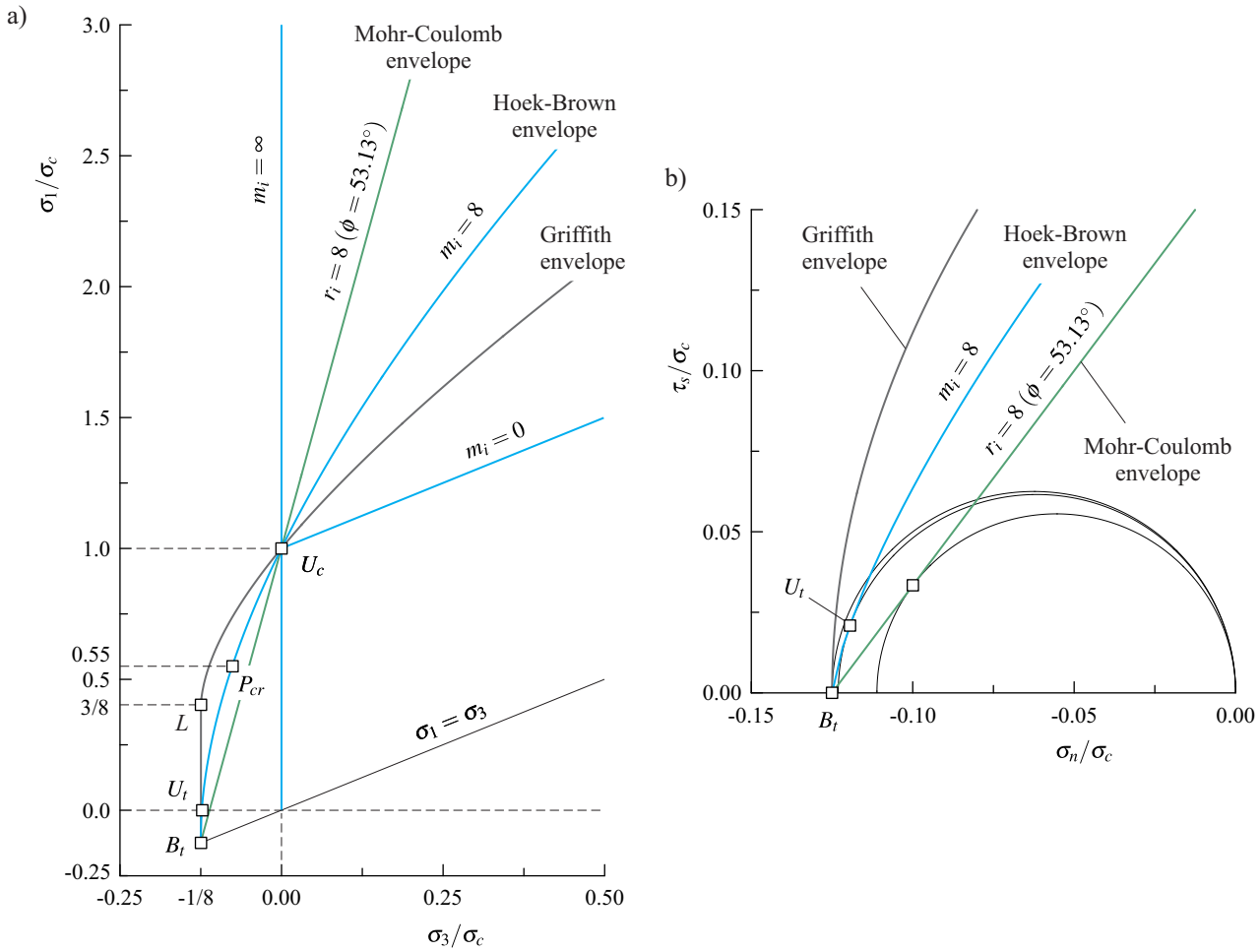

Figure 4. Hoek-Brown failure criterion for different compression-to-tension strength ratios, m_i, expressed in terms of a) principal stresses and b) stresses on the failure plane. Griffith and Mohr-Coulomb failure criteria are included for comparison.

For the first case, the resulting failure criterion is obtained by making $m_i = 0$ in equation (30), i.e.,

$$\frac{\sigma_1}{\sigma_c} = \frac{\sigma_3}{\sigma_c} + 1 \tag{34}$$

which corresponds to the failure criterion of a frictionless (cohesive only) material —and therefore to a failure envelope parallel to the bisector line $\sigma_1 = \sigma_3$ in Figure 4a.

For the second case, the resulting failure criterion is obtained by taking the limit when m_i tends to ∞ in equation (30), i.e.,

$$\frac{\sigma_1}{\sigma_c} \to \infty \tag{35}$$

which means that when the ratio of biaxial tensile strength and compressive strength is zero, the predicted major principal stress at failure is unbounded —and the failure envelope becomes a vertical line, as represented in Figure 4a.

Figure 4a shows the points B_t and U_t (see also Figure 1a) for the failure envelope corresponding to $m_i = 8$. According to the first observation made in Section 2.1, for the Hoek-Brown failure criterion (as well as for

the Mohr-Coulomb failure criterion discussed in Section 2.2) these points do not align vertically, and the uniaxial tensile strength (σ_{tUx}) associated with point U_t is smaller, in absolute value, than the biaxial tensile strength (σ_{tBx}) associated with point B_t. Indeed, making $\sigma_3 = \sigma_{tUx}$ and $\sigma_1 = 0$ in equation (30), the uniaxial tensile strength divided by σ_c is

$$\frac{\sigma_{tUx}}{\sigma_c} = -\frac{\sqrt{m_i^2+4}-m_i}{2} \tag{36}$$

and therefore, considering the second equation (31),

$$\frac{\sigma_{tUx}}{\sigma_{tBx}} < 1 \tag{37}$$

In view of equation (37), the Hoek-Brown failure criterion requires a tension cut-off at point U_t or at a point to the right of U_t in Figure 4a. The need of a tension cut-off in the Hoek-Brown failure criterion has been suggested in recent publications (Hoek & Martin 2014; Hoek & Brown 2019).

The Hoek-Brown failure criterion cannot be written in terms of stresses on the failure plane using a simple power law function as in equation (12) —at least not when the Hoek-Brown failure criterion considers the coefficient E in equation (8) to be null. This is in contrast with an early postulate that the Hoek-Brown failure criterion allowed such simple power law form —see Hoek & Brown (1980a). Therefore the Hoek-Brown failure criterion is not a particular case of the general power law failure criterion expressed in terms of stresses on the failure plane proposed in this paper.

The recasting of the Hoek-Brown failure criterion expressed in term of stresses on the failure plane can be done using the set of equations (10) and (11). Figure 4b shows the resulting Hoek-Brown failure envelope for the case $m_i = 8$ represented in Figure 4a. Figure 4b also includes the Griffith failure envelope and the Mohr-Coulomb failure envelope corresponding to $r_i = 8$. Figure 4b shows that the Hoek-Brown failure envelope is an *intermediate* failure envelope that lies in between the Griffith and Mohr-Coulomb failure envelopes.

2.4. The Fairhurst failure criterion

When discussing the need to apply a tension cut-off to the Hoek-Brown failure criterion, Hoek & Martin (2014) refer to the so called Fairhurst failure criterion, that has the particularity of points U_t and B_t in Figure 1a being aligned vertically; this means that the uniaxial tensile strength, σ_{tUx}, is equal to the biaxial tensile strength, σ_{tBx}.

The Fairhurst failure criterion is the generalization of the Griffith failure criterion for a variable ratio of unconfined compression strength and tensile strength. The equations conforming the criterion were first published in Fairhurst (1964). In this section, a rewritten version of the original equations are provided. The Fairhurst failure criterion includes the unconfined compressive strength, σ_c, and a parameter designated here as the n_i parameter as the main rock parameters in the failure criterion. The parameter n_i represents the ratio of unconfined compression strength and tensile strength, and therefore it is comparable to the parameter m_i in the Hoek-Brown failure criterion, and the parameter r_i in the Mohr-Coulomb failure criterion.

The Fairhurst failure criterion expressed in terms of principal stresses σ_1 and σ_3 is as follows

$$\frac{\sigma_1}{\sigma_c} = \frac{\sigma_3}{\sigma_c} + 2\frac{\sqrt{n_i+1}-1}{\sqrt{n_i}}\sqrt{\frac{\sigma_3}{\sigma_c}+\frac{1}{n_i}} + \frac{\left(\sqrt{n_i+1}-1\right)^2}{n_i} \quad \text{if} \quad \frac{\sigma_1}{\sigma_c} \geq \frac{\sigma_{1\mathrm{L}}}{\sigma_c} \tag{38}$$

and

$$\frac{\sigma_3}{\sigma_c} = -\frac{1}{n_i} \quad \text{if} \quad \frac{\sigma_1}{\sigma_c} \leq \frac{\sigma_{1L}}{\sigma_c} \tag{39}$$

As mentioned previously, the parameter n_i is

$$n_i = -\frac{\sigma_c}{\sigma_{tBx}} \tag{40}$$

and the scaled stress σ_{1L}/σ_c is

$$\frac{\sigma_{1L}}{\sigma_c} = \frac{\left(\sqrt{n_i+1}-2\right)\sqrt{n_i+1}}{n_i} \tag{41}$$

When the parameter n_i is considered to be equal to 8 in equations (38) through (41), these equations become the very same equations (1) and (2) for the Griffith failure criterion.

In view of equation (40), the Fairhurst failure criterion can also be written as follows

$$\frac{\sigma_1}{\sigma_c} = \frac{\sigma_3}{\sigma_c} + 2\frac{\sqrt{n_i+1}-1}{\sqrt{n_i}}\sqrt{\frac{\sigma_3}{\sigma_c} - \frac{\sigma_{tBx}}{\sigma_c}} + \frac{\left(\sqrt{n_i+1}-1\right)^2}{n_i} \quad \text{if} \quad \frac{\sigma_1}{\sigma_c} \geq \frac{\sigma_{1L}}{\sigma_c} \tag{42}$$

Comparing equation (42) with equation (8), the Fairhurst failure criterion is found to be a particular case of the general power law failure criterion given by equation (8) when

$$C = 2\frac{\sqrt{n_i+1}-1}{\sqrt{n_i}} \qquad D = \frac{1}{2} \quad \text{and} \quad E = \frac{\left(\sqrt{n_i+1}-1\right)^2}{n_i} \tag{43}$$

with these constants also satisfying the equation (9).

The Faihrust failure criterion given by equations (38) through (41) is represented graphically Figure 5a. The diagram includes different failure envelopes corresponding to different values of the parameter n_i. As a reference, the Hoek-Brown failure envelope for $m_i = 8$ is also represented in Figure 5a. As already discussed in Section 2.3, when compared with the Hoek-Brown failure criterion for $m_i = 8$, the Griffith failure criterion (or Fairhurst failure criterion for $n_i = 8$) predicts lower values of major principal stresses at failure in the confined compressive stress regime, and larger values of major principal stresses at failure in the confined tensile stress regime.

Figure 5a includes the Fairhurst failure envelopes for two limiting cases of the ratio n_i, namely $n_i = 0$ and $n_i = \infty$.

For the first case, the resulting failure criterion is obtained by taking the limit when n_i tends to 0 in the first of equations (38), i.e.,

$$\frac{\sigma_1}{\sigma_c} = \frac{\sigma_3}{\sigma_c} + 1 \tag{44}$$

which corresponds to the failure criterion of a frictionless (cohesive only) material —and therefore to a failure envelope parallel to the bisector line $\sigma_1 = \sigma_3$ in Figure 5a.

For the second case, the resulting failure criterion is obtained by taking the limit when n_i tends to ∞ in the

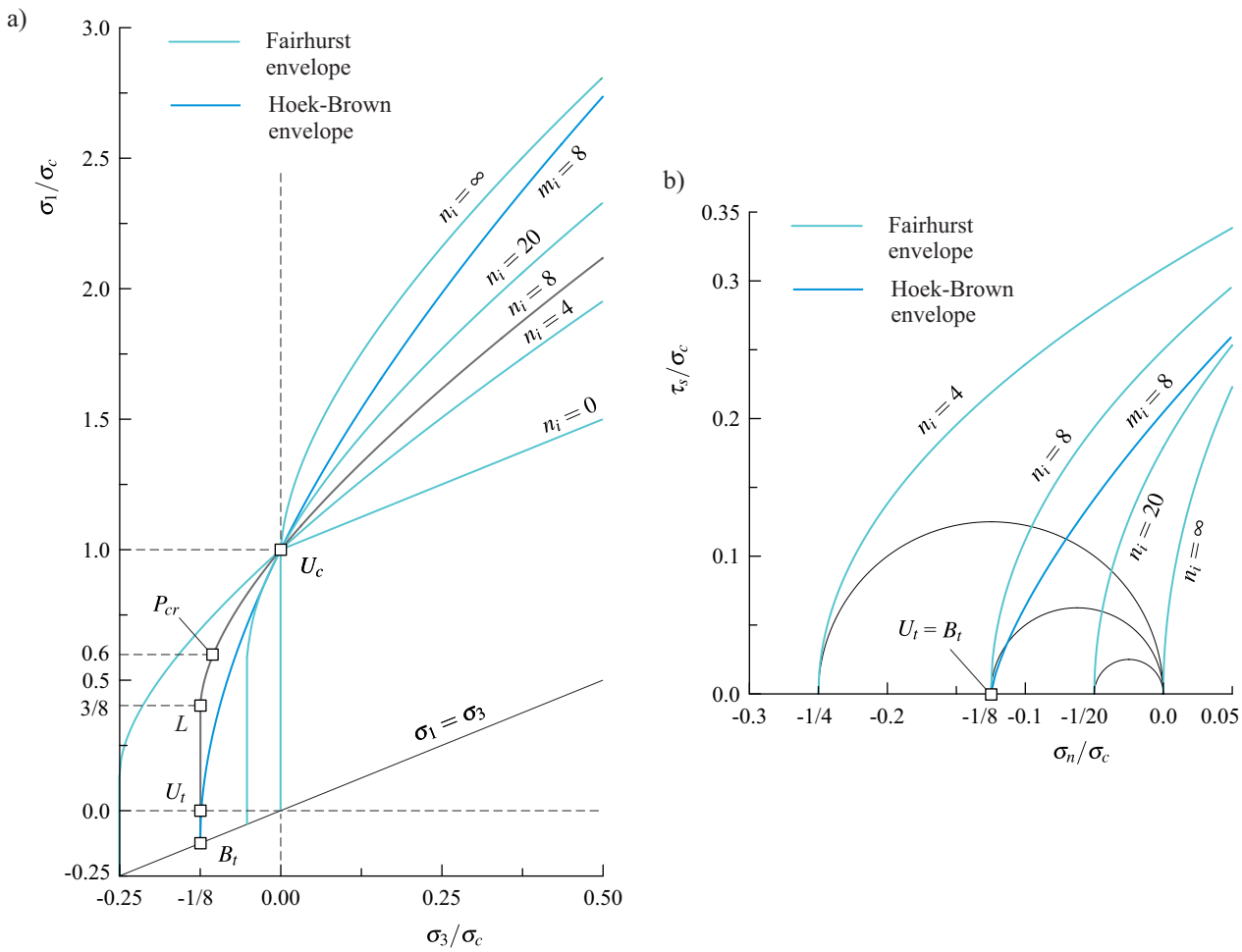

Figure 5. Fairhurst failure criterion for different compression-to-tension strength ratios, n_i, expressed in terms of a) principal stresses and b) stresses on the failure plane. The Hoek-Brown failure criterion is included for comparison.

first of equations (38). This limit results

$$\frac{\sigma_1}{\sigma_c} = \frac{\sigma_3}{\sigma_c} + 2\sqrt{\frac{\sigma_3}{\sigma_c}} + 1 \tag{45}$$

which means that when the ratio of biaxial tensile strength and compressive strength is zero, the predicted major principal strength is now bounded to an upper limiting envelope. This is in contrast with the Mohr-Coulomb and Hoek-Brown failure envelopes discussed in Sections 2.2 and 2.3, respectively.

Figure 5a shows the points B_t and U_t (see also Figure 1a) for the Fairhurst failure envelope corresponding to $n_i = 8$. As mentioned previously, the points are aligned vertically. This will be the case provided the stress σ_{1L}/σ_c is above the horizontal axis. In that case, equation (40) can be written as follows

$$n_i = -\frac{\sigma_c}{\sigma_{tBx}} = -\frac{\sigma_c}{\sigma_{tUx}} \tag{46}$$

Making $\sigma_{1L}/\sigma_c \geq 0$ in equation (41), the points B_t and U_t will be aligned vertically provided $n_i \geq 3$. If $n_i < 3$, the Fairhurst failure criterion requires a tension cut-off, as in the case of the Mohr-Coulomb and Hoek-Brown failure criteria.

The Fairhurst failure criterion expressed in terms of normal and shear stresses (divided by the unconfined compressive strength) can be written as follows (Fairhurst 1964)

$$\frac{\tau_s}{\sigma_c} = \sqrt{\frac{2\left(1-\sqrt{n_i+1}\right)+n_i}{n_i}}\sqrt{\frac{\sigma_n}{\sigma_c}-\frac{\sigma_{tBx}}{\sigma_c}} \tag{47}$$

Comparing equation (47) with equation (12), the constants A and B in equation (12) result to be

$$A = \sqrt{\frac{2\left(1-\sqrt{n_i+1}\right)+n_i}{n_i}} \quad \text{and} \quad B = \frac{1}{2} \tag{48}$$

In view of equations (42) and (47), the Fairhurst failure criterion is therefore shown to be a particular case of the general power law failure criteria expressed in terms of principal stresses (equation 8) and in terms of stresses on the failure plane (equation 12), respectively.

Finally, equation (47) is represented graphically in Figure 5b for the same values of the coefficients n_i in Figure 5a —the Hoek-Brown failure criterion is also included as a reference. As expected, the origin of the various failure envelopes are located at the abscisas corresponding to the $1/n_i$ values.

3. SCALING OF POWER LAW FAILURE CRITERIA FOR INTACT ROCK

3.1. Scaling of the general form of the power law failure criterion

The general power law failure criteria given by equations (8) and (12) allow scaled forms that can bring advantages in the interpretation of problems involving the failure criteria, as it will be illustrated with application examples later on in this paper.

For the general power law failure criterion expressed in terms of principal stresses (equation 8), the scaled form that applies when $0.5 \leq D < 1$ is

$$S_1 = S_3 + S_3^D + E\,C^{-1/(1-D)} \tag{49}$$

where

$$S_1 = \left(\frac{\sigma_1}{\sigma_c} - \frac{\sigma_{tBx}}{\sigma_c}\right) C^{-1/(1-D)} \quad \text{and} \quad S_3 = \left(\frac{\sigma_3}{\sigma_c} - \frac{\sigma_{tBx}}{\sigma_c}\right) C^{-1/(1-D)} \tag{50}$$

and when $D = 1$, it is

$$S_1 = (C+1)S_3 \tag{51}$$

where

$$S_1 = \frac{\sigma_1}{\sigma_c} - \frac{\sigma_{tBx}}{\sigma_c} + \frac{E}{C} \quad \text{and} \quad S_3 = \frac{\sigma_3}{\sigma_c} - \frac{\sigma_{tBx}}{\sigma_c} + \frac{E}{C} \tag{52}$$

For the general power law failure criterion expressed in terms of stresses on the failure plane (equation 12), the scaled form that applies when $0.5 \leq B < 1$ is

$$T_s = S_n^B \tag{53}$$

where

$$T_s = \frac{\tau_s}{\sigma_c} A^{-1/(1-B)} \quad \text{and} \quad S_n = \left(\frac{\sigma_n}{\sigma_c} - \frac{\sigma_{tBx}}{\sigma_c} \right) A^{-1/(1-B)} \tag{54}$$

and when $B = 1$, it is

$$T_s = A\, S_n \tag{55}$$

where

$$T_s = \frac{\tau_s}{\sigma_c} \quad \text{and} \quad S_n = \frac{\sigma_n}{\sigma_c} - \frac{\sigma_{tBx}}{\sigma_c} A^{-1} \tag{56}$$

The following sections provide the particular forms that the equations above take, for the particular cases of the general power law failure criteria corresponding to the Mohr-Coulomb, Hoek-Brown and Fairhurst failure criteria.

3.2. Scaling of the Mohr-Coulomb failure criterion

According to Section 2.2, the Mohr-Coulomb failure criterion expressed in terms of principal stresses is a particular case of the general power law failure criterion (equation 8) when $C = r_i$, $D = 1$ and $E = 0$. Considering also that σ_{tBx}/σ_c is related to the parameter r_i according to equation (17), equations (51) and (52) become

$$S_1 = (r_i + 1) S_3 \tag{57}$$

and

$$S_1 = \frac{\sigma_1}{\sigma_c} + \frac{1}{r_i}; \qquad S_3 = \frac{\sigma_3}{\sigma_c} + \frac{1}{r_i} \tag{58}$$

Also, according to Section 2.2, the Mohr-Coulomb failure criterion expressed in terms of stresses on the failure plane is a particular case of the general power law failure criterion (equation 12) when $A = r_i/(2\sqrt{r_i + 1})$ and $B = 1$ (with σ_{tBx}/σ_c related to r_i according to equation 17). Therefore, equations (55) and (56) become

$$T_s = \frac{r_i}{2\sqrt{r_i + 1}} S_n \tag{59}$$

and

$$T_s = \frac{\tau_s}{\sigma_c}; \qquad S_n = \frac{\sigma_n}{\sigma_c} + \frac{2\sqrt{r_i + 1}}{r_i^2} \tag{60}$$

The scaled form of the Mohr-Coulomb failure criteria above has been known and used by several authors in the past. For example, equations (59) and (60) were used by Hoek & Bray (1981) to produce dimensionless representations of stability charts for rock slopes assuming circular failure surface based on limit equilibrium models. Equations (57) and (58) were used by Carranza-Torres (2003) to produce dimensionless representations of ground reaction curves for the convergence confinement method of tunnel support design, based on elasto-plastic models.

3.3. Scaling of the Hoek-Brown failure criterion

According to Section 2.3, the Hoek-Brown failure criterion for intact rock is a particular case of the general power law failure criterion when the coefficients C, D and E are given by equations (33). Considering that σ_{tBx}/σ_c is related to the coefficient m_i by equations (31), equations (49) and (50) become

$$S_1 = S_3 + \sqrt{S_3} \tag{61}$$

and

$$S_1 = \left(\frac{\sigma_1}{\sigma_c} + \frac{1}{m_i}\right)\frac{1}{m_i}; \qquad S_3 = \left(\frac{\sigma_3}{\sigma_c} + \frac{1}{m_i}\right)\frac{1}{m_i} \tag{62}$$

Equations (61) and (62) correspond to the scaled version of the Hoek-Brown failure criterion for intact rock proposed by Londe (1988).

To illustrate the use of equations (61) and (62), Figure 6a represents the selected cases of uniaxial and triaxial compression test results from Figure 3, designated as Cases 2, 10, 11, 15 and 17, together with the corresponding computed best fit Hoek-Brown failure envelopes. Figure 6b represents the same test results, after the scaling in equations (62) has been applied. Points corresponding to different rock types that are aligned to their corresponding failure envelopes in Figure 6a, appear now aligned to a unique scaled Hoek-Brown failure envelope given by equation (61). Table 1 includes the data represented in Figure 6.

Although this section focuses primarily on failure criteria for intact rock, the generalized Hoek-Brown failure criterion that applies to rock masses is also a particular case of the power law failure criterion introduced in Section 2.1, and therefore also allows a scaled form as given by equations (49) and (50). Because of the significance of the generalized Hoek-Brown failure criterion in practical rock engineering, details of the scaling of this failure criterion are provided in Appendix B.

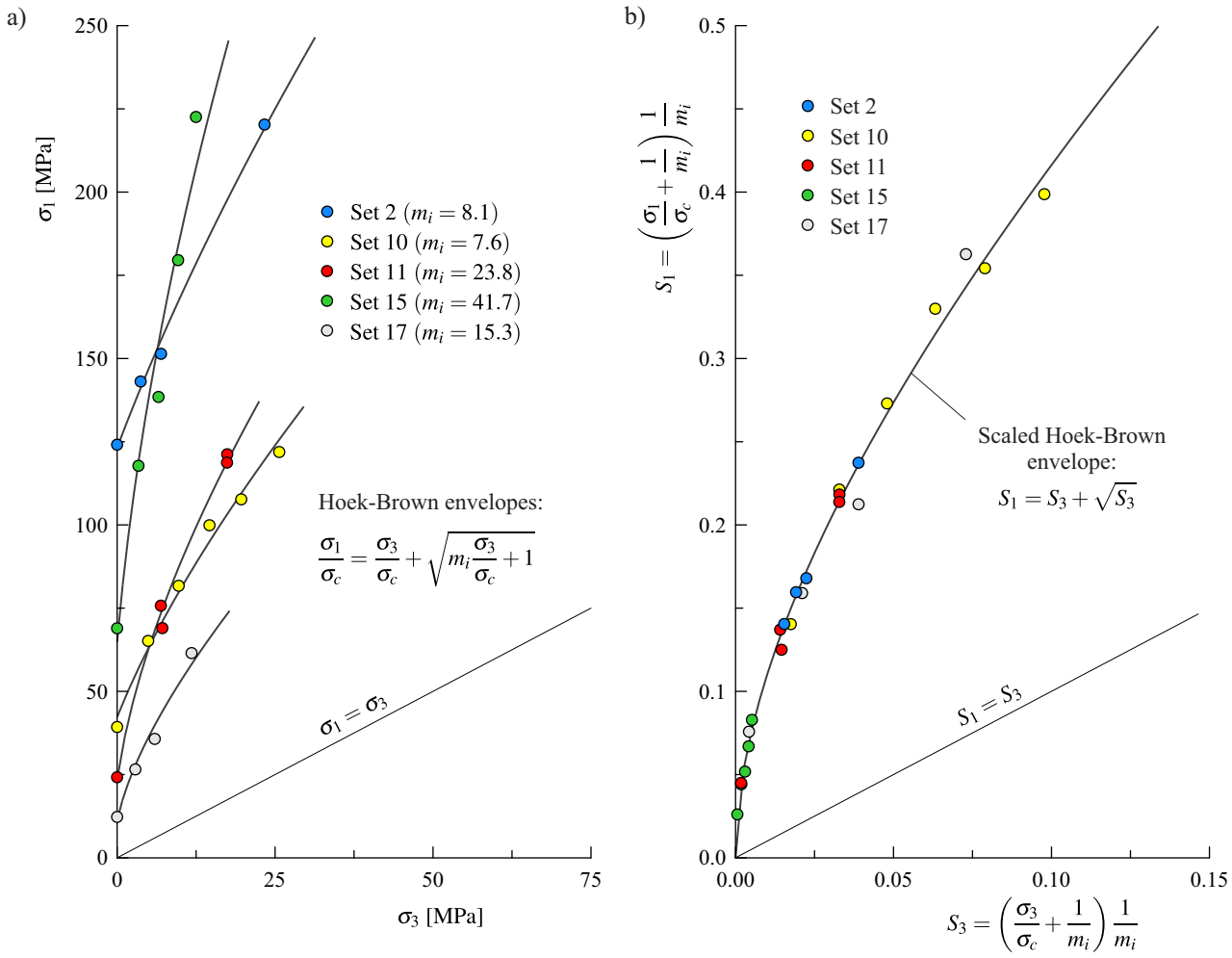

Figure 6. a) Selected cases of uniaxial and triaxial compression test results from Figure 3, together with the corresponding best fit Hoek-Brown failure envelopes. b) Same test results expressed in terms of scaled principal stresses.

Table 1. Summary of uniaxial and triaxial test results represented in Figure 6.

Set	σ_3 [MPa]	σ_1 [MPa]	m_i [-]	σ_c [MPa]	S_3 [-]	S_1 [-]
2	0.00	124.11	8.1	123.21	0.0154	0.1405
	3.72	143.09			0.0192	0.1596
	6.95	151.41			0.0224	0.1680
	23.33	220.29			0.0389	0.2374
10	0.00	39.30	7.6	42.28	0.0175	0.1404
	4.91	65.16			0.0328	0.2213
	9.75	81.71			0.0480	0.2730
	14.62	99.90			0.0632	0.3299
	19.65	107.68			0.0789	0.3542
	25.66	121.91			0.0977	0.3987
11	0.00	24.20	23.8	23.52	0.0018	0.0450
	7.16	69.00			0.0146	0.1250
	6.92	75.75			0.0141	0.1371
	17.40	118.73			0.0328	0.2138
	17.42	121.22			0.0329	0.2183
15	0.00	68.95	41.7	64.79	0.0006	0.0261
	3.38	117.76			0.0018	0.0441
	6.55	138.45			0.0030	0.0518
	9.65	179.54			0.0041	0.0670
	12.48	222.56			0.0052	0.0829
17	0.00	12.27	15.3	11.19	0.0043	0.0758
	2.88	26.56			0.0211	0.1590
	5.95	35.71			0.0389	0.2124
	11.78	61.50			0.0729	0.3627

3.4. Scaling of the Fairhurst failure criterion

According to Section 2.4, the Fairhurst failure criterion for intact rock is a particular case of the general power law failure criterion (equation 8) when the coefficients C, D and E are given by equations (43). Considering that σ_{tBx}/σ_c is related to the coefficient n_i by equation (40), equations (49) and (50) become

$$S_1 = S_3 + \sqrt{S_3} + \frac{1}{4} \qquad \text{if} \qquad S_1 \geq 1/4 \tag{63}$$

$$S_3 = 0 \qquad \text{if} \qquad S_1 \leq 1/4 \tag{64}$$

$$S_1 = \left(\frac{\sigma_1}{\sigma_c} + \frac{1}{n_i}\right) \frac{n_i}{4\left(\sqrt{n_i+1}-1\right)^2}; \qquad S_3 = \left(\frac{\sigma_3}{\sigma_c} + \frac{1}{n_i}\right) \frac{n_i}{4\left(\sqrt{n_i+1}-1\right)^2} \tag{65}$$

Also, according to Section 2.4, the Fairhurst failure criterion expressed in terms of stresses on the failure plane is a particular case of the general power law failure criterion (equation 12) when the coefficients A and B are given by equations (48). Considering that σ_{tBx}/σ_c is also related to n_i according to equation (40), equations (53) and (54) become

$$T_s = \sqrt{S_n} \tag{66}$$

where

$$T_s = \frac{\tau_s}{\sigma_c} \frac{n_i}{2\left(1-\sqrt{n_i+1}\right)+n_i} \qquad \text{and} \qquad S_n = \left(\frac{\sigma_n}{\sigma_c}+\frac{1}{n_i}\right) \frac{n_i}{2\left(1-\sqrt{n_i+1}\right)+n_i} \tag{67}$$

To illustrate the use of equations (63) through (65), the dots in Figure 7a represent test results corresponding to three different rock types obeying the Fairhurst failure criterion. Set A corresponds to (mostly) tensile strength test results reported by Hoek & Martin (2014), and originally published by Ramsey & Chester (2004). Sets B and C are synthetic (or artificial) tests results generated for purposes of illustration. Figure 7a also includes the best fit Fairhurst failure envelopes computed for the three sets. Figure 7b represents the same test results, after the scaling in equations (65) has been applied. Points corresponding to the different rock types that are aligned to their corresponding failure envelopes in Figure 7a, appear now aligned to a unique scaled Fairhurst failure envelope given by equations (63) and (64). Table 2 includes the data represented in Figure 7.

Finally, it should be noticed that the scaled form of the Griffith failure criterion is also given by the equations presented in this section, when the parameter n_i is considered to be equal to 8.

4. POWER LAW FAILURE CRITERION FOR UNCEMENTED ROCKFILL INTERFACES

Shear strength of uncemented rockfill interfaces has been traditionally determined from direct shear testing or from triaxial testing of large samples of rockfill —see, for example, Marsal (1967); Marachi et al. (1972); Linero et al. (2007); Ovalle et al. (2020). Although the Mohr-Coulomb linear failure criterion has been applied to fit test results, power law failure criteria such as those proposed by de de Mello (1977) and by Indraratna et al. (1993), introduced in Section 1, show better agreement with test results. In this section, the latter failure criterion will be considered. As discussed in Section 1, for the Indraratna et al. failure criterion the relationship between shear and normal stresses for an uncemented rockfill interface takes the form

$$\frac{\tau_s}{\sigma_{cF}} = A\left(\frac{\sigma_n}{\sigma_{cF}}\right)^B \tag{68}$$

where A and B are constants, and σ_{cF} is a representative average of the unconfined compressive strength of the rock fragments.

If the constant A is moved to the right side in equation (68), the Indraratna et al. failure criterion can be represented graphically as shown in Figure 8. The diagram in Figure 8 considers three distinct values for the constant B, namely 0.5, 0.75 and 1.0. As discussed in Section 2.1, the variable B must be lie between 0.5 and 1.

Comparing equation (68) with equation (12), the Indraratna et al. failure criterion for uncemented rockfill can be regarded as a particular case of the general power law failure criterion introduced in Section 2.1, except that the unconfined compression strength of the rock, σ_c, is replaced with the unconfined compression strength of the rock fragments, σ_{cF}, and the tensile strength is assumed zero.

To understand the influence of the unconfined compressive strength of the rock fragments (σ_{cF}) in the strength of the rockfill, equation will be rewritten assuming the properties A, B and σ_{cF} in equation (68), are now *measured* properties A^*, B^* and σ^*_{cF}, respectively, obtained from laboratory testing of the rockfill (i.e., A^* and B^* from triaxial testing or from direct shear testing of the rock fill interface, and σ^*_{cF} from unconfined compression tests of the rock fragments). Assuming this notation, equation (68) is now written

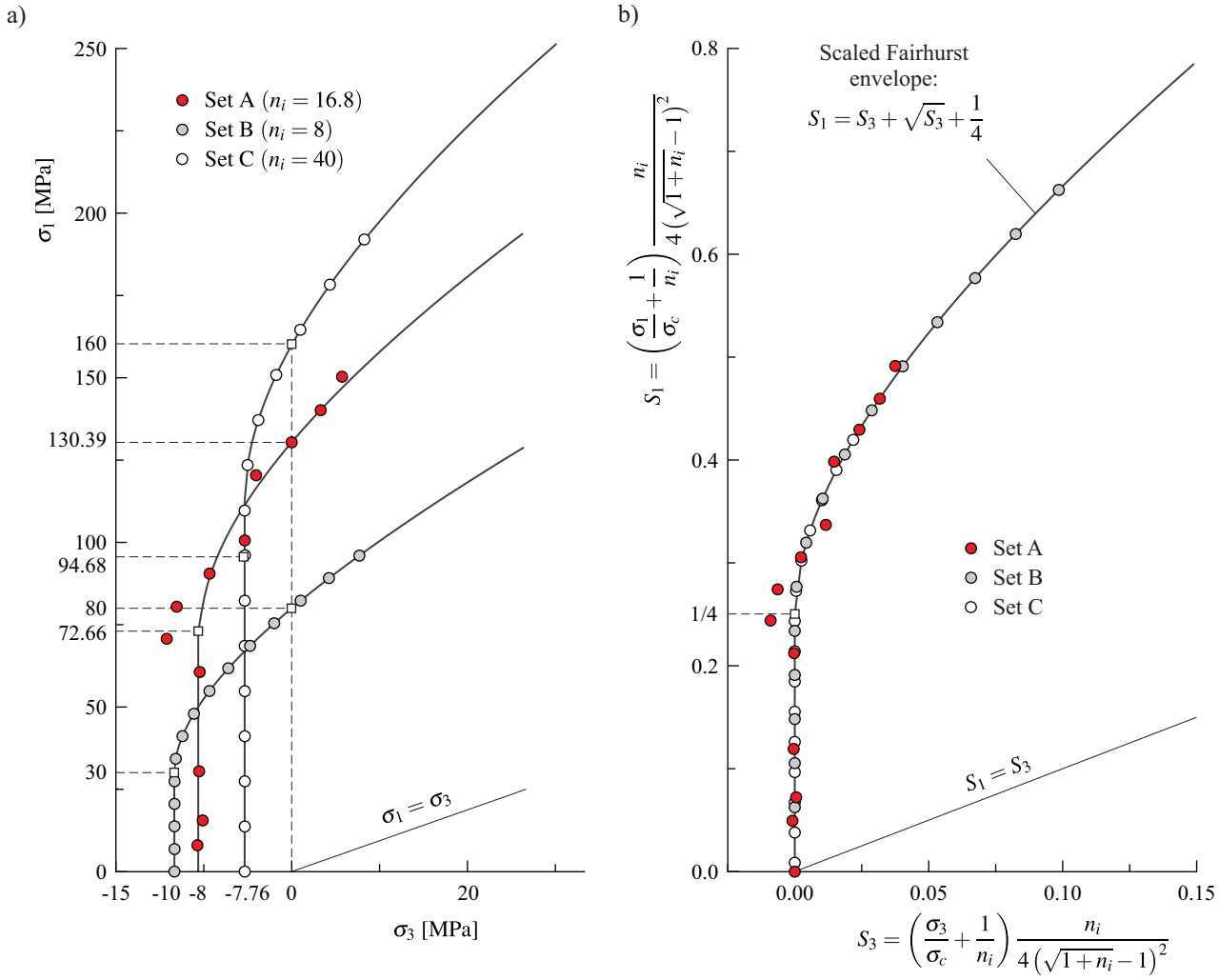

Figure 7. a) Direct tension test results reported in Hoek & Martin (2014) (Set A) and synthetic test results (Sets B and C), together with the corresponding best fit Fairhurst failure envelopes. b) Same test results expressed in terms of scaled principal stresses.

Table 2. Summary of strength test results represented in Figure 7.

Set	σ_3 [MPa]	σ_1 [MPa]	n_i [-]	σ_c [MPa]	σ_{1L} [MPa]	σ_{tUx} [MPa]	S_3 [-]	S_1 [-]
A	-8.04	8.12	16.8	130.39	72.66	-7.76	-0.0009	0.0494
	-7.59	15.45					0.0005	0.0722
	-7.89	30.58					-0.0004	0.1192
	-7.84	60.53					-0.0002	0.2123
	-10.66	70.72					-0.0090	0.2440
	-9.81	80.46					-0.0064	0.2742
	-7.01	90.52					0.0023	0.3055
	-4.03	100.63					0.0116	0.3369
	-3.04	120.40					0.0147	0.3984
	0.00	130.39					0.0241	0.4295
	2.45	140.09					0.0317	0.4596
	4.30	150.32					0.0375	0.4914
B	-10.00	0.00	8	80.00	30.00	-10.00	0.0000	0.0625
	-10.00	13.71					0.0000	0.1482
	-10.00	27.43					0.0000	0.2339
	-9.89	34.29					0.0007	0.2768
	-8.33	48.00					0.0104	0.3625
	-5.40	61.71					0.0287	0.4482
	-1.48	75.43					0.0532	0.5339
	3.20	89.14					0.0825	0.6196
C	-4.00	0.00	40	160.00	94.68	-8.00	0.0000	0.0086
	-4.00	27.43					0.0000	0.0673
	-4.00	54.86					0.0000	0.1260
	-4.00	82.29					0.0000	0.1847
	-4.00	109.71					0.0000	0.2434
	-3.77	123.43					0.0005	0.2728
	-1.32	150.86					0.0057	0.3315
	3.26	178.29					0.0156	0.3902

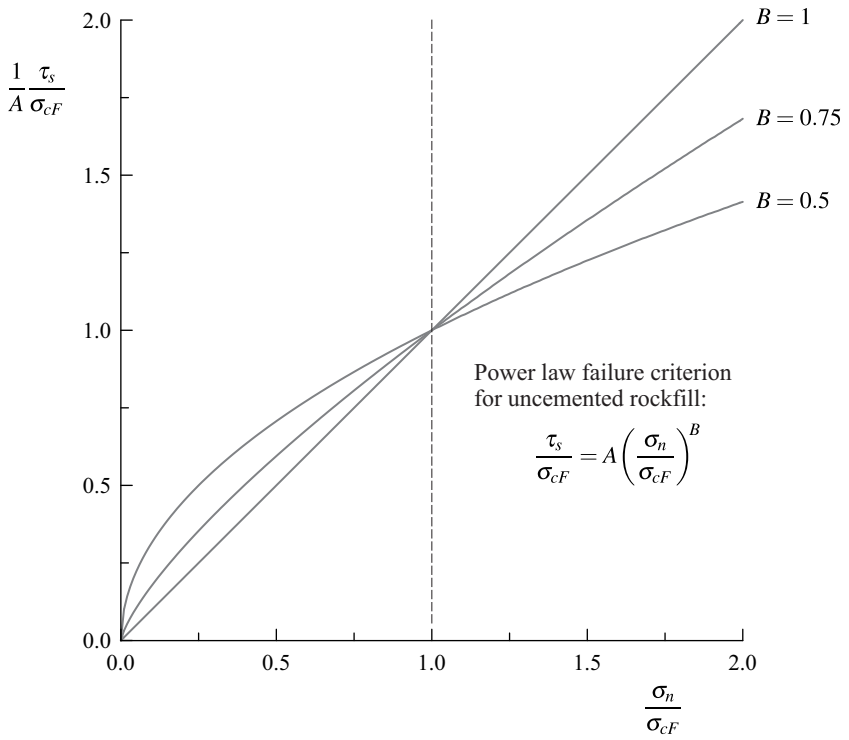

Figure 8. Scaled representation of the Indraratna et al. failure criterion for uncemented rock fill.

as follows

$$\frac{\tau_s}{\sigma^*_{cF}} = A^*\left(\frac{\sigma_n}{\sigma^*_{cF}}\right)^{B^*} \tag{69}$$

Considering a rockfill that has the same constants A^* and B^* measured in the lab but an arbitrary unconfined compressive strength of rock fragments, σ_{cF}, the expected shear strength, τ_s, for the same value of normal stress, σ_n, will be different from the one corresponding to the rockfill tested in the lab, i.e.,

$$\tau_s\left(\sigma_n, A^*, B^*, \sigma_{cF}\right) \neq \tau_s\left(\sigma_n, A^*, B^*, \sigma^*_{cF}\right) \tag{70}$$

In view of equations (68) and (69), the ratio of shear strengths for the rockfill with unconfined compression strength of fragments (σ_{cF}) and the one with measured unconfined compression strength (σ^*_{cF}) will be

$$r_{\tau s} = \frac{\tau_s\left(\sigma_n, A, B^*, \sigma_{cF}\right)}{\tau_s\left(\sigma_n, A^*, B^*, \sigma^*_{cF}\right)} = \frac{A}{A^*}\frac{\sigma_{cF}}{\sigma^*_{cF}}\left(\frac{\sigma^*_{cF}}{\sigma_{cF}}\right)^{B^*} \tag{71}$$

Figure 9 represents the shear strength ratio given by equation (71) for three different values of the constant B^* (assumed to be the same as B), namely 0.5, 0.75 and 1.0. The lines in Figure 9 shows that if the unconfined compressive strength of the rockfill fragments (σ_{cF}) is the same as the measured in the lab (σ^*_{cF}), then the shear strength of the rockfill interface will be the same. If $\sigma_{cF} < \sigma^*_{cF}$, the predicted shear strength will be lower, and if $\sigma_{cF} > \sigma^*_{cF}$, the predicted shear strength will be higher than the one corresponding to the tested rockfill (this being the case if $B^* > 1$; if $B^* = 1$, σ_{cF} will not have any effect on the shear strength of the interface). The points labelled as C_1, C_{1a} and C_{1d} correspond to cases that will be discussed later on, in an

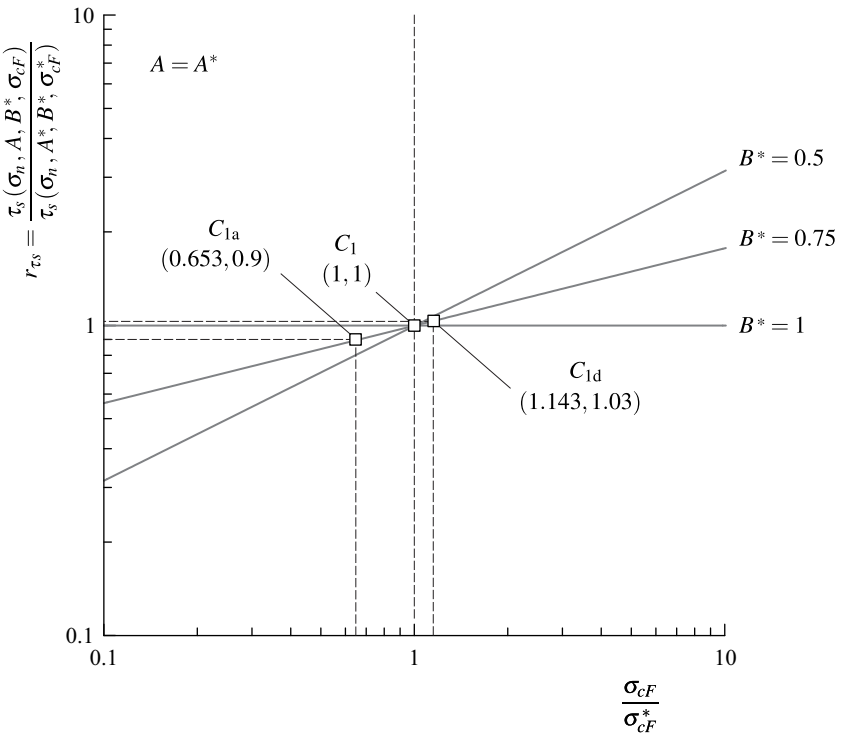

Figure 9. Graphical representation of the relationship between the shear strength ratio, $r_{\tau s}$, and the ratio of unconfined compressive strength, σ_{cF}, and *measured* unconfined compressive strength, σ^*_{cF}.

example involving rockfill slopes in Section 6.2.

The dependence of σ^*_{cF} on the shear strength of the rockfill interface given by equation (69) is the *natural* dependence embedded in the Indraratna et al. failure criterion. If the case of another rockill is considered where σ_{cF} and the ratio $r_{\tau s}$ (for a certain normal stress) are known, a corrected value of the constant A can be found with the following equation, obtained by rearranging terms in equation (71),

$$A = r_{\tau s}\, A^* \frac{\sigma^*_{cF}}{\sigma_{cF}} \left(\frac{\sigma_{cF}}{\sigma^*_{cF}} \right)^{B^*} \tag{72}$$

A scaled version of the Indraratna et al. failure criterion given by equation (68) can be obtained with the scaling rules introduced in Section 3.1.

For the case $0.5 \leq B < 1$ the scaled failure criterion is

$$T_s = S_n^B \tag{73}$$

where

$$T_s = \frac{\tau_s}{\sigma_{cF}} A^{-1/(1-B)} \quad \text{and} \quad S_n = \frac{\sigma_n}{\sigma_{cF}} A^{-1/(1-B)} \tag{74}$$

For the case $B = 1$ the scaled failure criterion is

$$T_s = A\, S_n \tag{75}$$

where

$$T_s = \frac{\tau_s}{\sigma_{cF}} \quad \text{and} \quad S_n = \frac{\sigma_n}{\sigma_{cF}} \tag{76}$$

To illustrate the use of equations (73) through (76), the dots in Figure 10a represent triaxial test results performed on large samples of three different rockfill types, designated as Sets D, E and F. All three rockfill types are characterized by the same constant $B^* = 0.75$. Figure 10a includes the best fit failure envelopes obtained with equations (13) and (14). Figure 10b represents the same test results, but expressed in terms of shear and normal stresses on the rockfill interface (this representation is the equivalent to the representation in Figure 10a, and has been obtained by application of equation 69). Figure 11 represents the same test results after the scaling in equations (74) has been applied. Points corresponding to the different rockfill types that are aligned to their corresponding failure envelopes in Figure 10, appear now aligned to a unique scaled power law failure envelope given by equation (73), corresponding to the measured value $B^* = 0.75$. Table 3 includes the data represented in Figures 10 and 11.

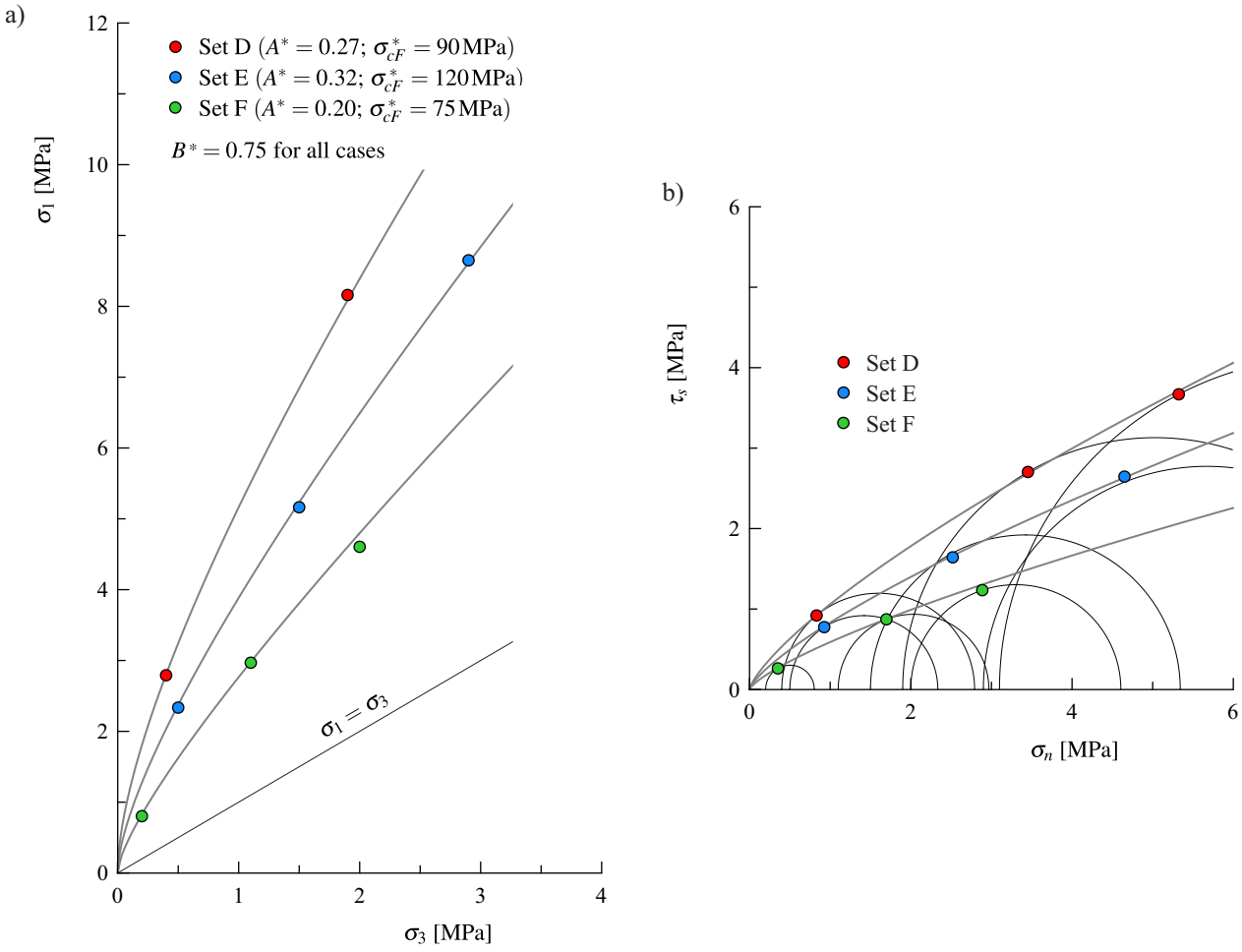

Figure 10. a) Results of triaxial compression tests on large samples of uncemented rockfill together with the corresponding best fit Indraratna et al. failure envelopes. b) Same test results expressed in terms of stresses on the failure plane.

Table 3. Summary of test results represented in Figures 10 and 11.

Set	σ_3 [MPa]	σ_1 [MPa]	σ_n [MPa]	τ_s [MPa]	A^* [-]	B^* [-]	σ^*_{cF} [MPa]	S_n [-]	T_s [-]
D	0.50	2.33	0.93	0.77	0.27	0.75	90.00	1.94	1.62
	1.50	5.16	2.52	1.64				5.27	3.43
	2.90	8.65	4.65	2.65				9.72	5.53
E	0.40	2.79	0.83	0.92	0.32	0.75	120.00	0.66	0.73
	1.90	8.16	3.45	2.70				2.74	2.15
	3.10	11.38	5.32	3.67				4.23	2.92
F	0.20	0.80	0.35	0.26	0.20	0.75	75.00	2.93	2.18
	1.10	2.97	1.70	0.87				14.15	7.26
	2.00	4.60	2.89	1.23				24.06	10.29

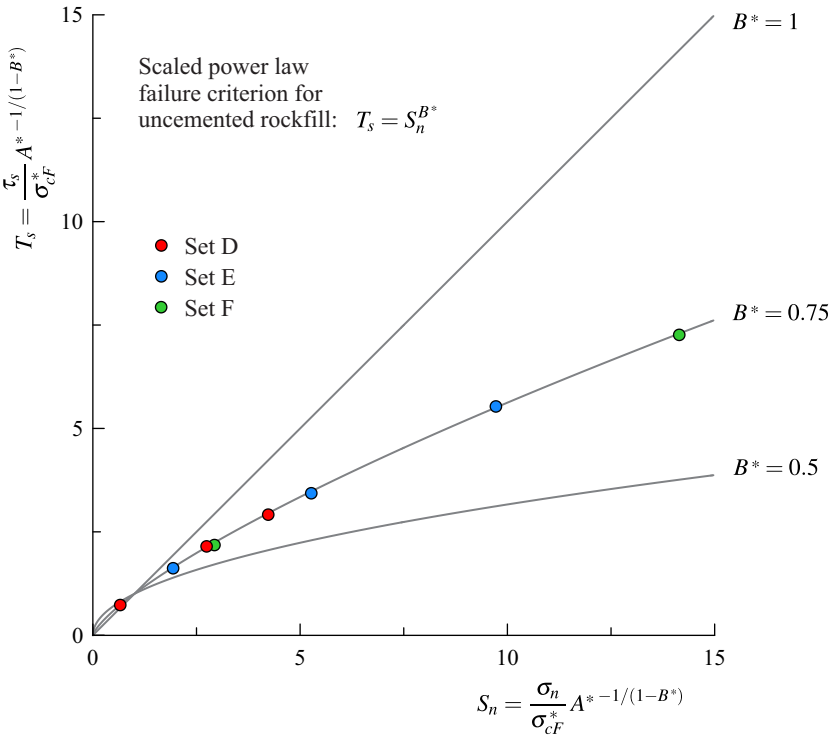

Figure 11. Same test results as in Figure 10, expressed in terms of scaled shear and normal stresses on the failure plane.

5. APPLICATION EXAMPLE 1: EXTENT OF DAMAGE AND WALL CONVERGENCE FOR A SECTION OF BOREHOLE DRIVEN IN INTACT ROCK

5.1. Problem statement

The first application example involves determining the extent of plastic failure and radial displacement of a plane-strain section of borehole assumed to be subjected to uniform (or hydrostatic) far-field stresses. The problem is schematically represented in Figure 12a. The borehole of radius R is driven in an assumed elasto-

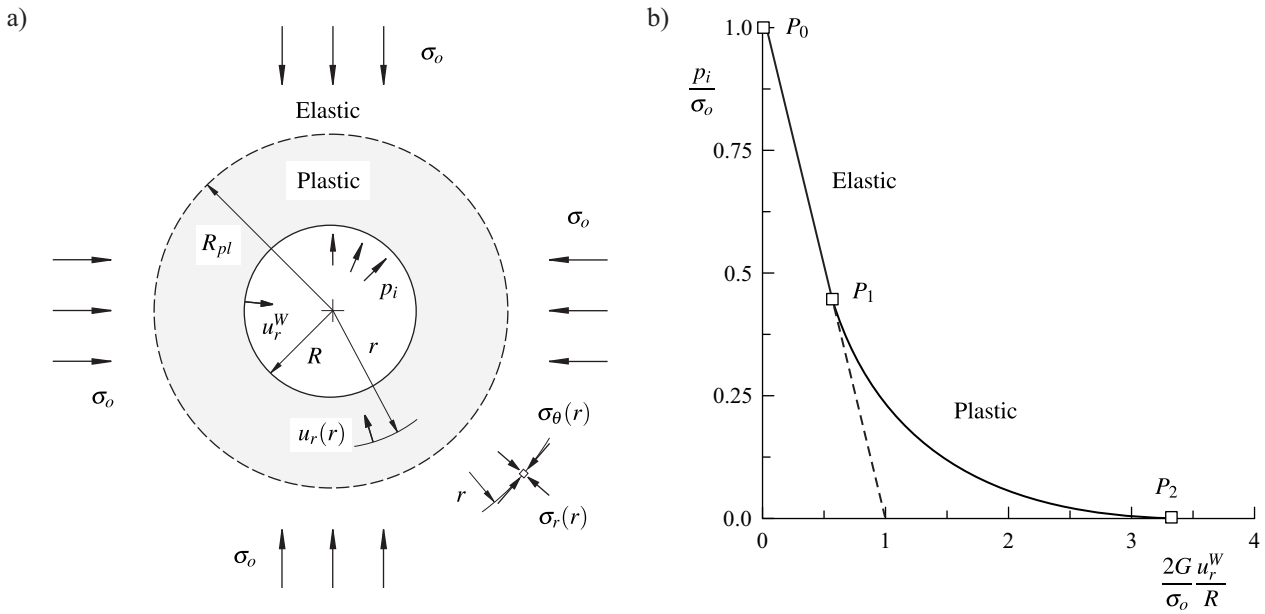

Figure 12. a) Elasto-plastic problem of section of circular borehole driven in intact rock. b) Ground reaction curve for the borehole.

plastic intact rock subjected to hydrostatic far-field stresses, σ_o. There is a uniform pressure, p_i, acting on the periphery of the hole. The rock is assumed to have an elastic shear modulus, G, and a Poisson's ratio, ν. The rock is also assumed to fail plastically, according to any of the failure criteria discussed in Section 2, and to have a constant dilation angle, ψ. When the internal pressure falls below a critical value p_i^{cr}, an annular region of radius R_{pl} develops around the hole. At a distance r from the hole center, the radial displacement is $u_r(r)$ and at the wall of the hole ($r = R$) the radial displacement is u_r^W. Radial displacements are positive when directed towards the hole center —see Figure 12a. Also, at a distance r, whether within the plastic region or the elastic region, the hoop stress, $\sigma_\theta(r)$, and the radial stress $\sigma_r(r)$ are major and minor principal stresses, respectively. Stresses are assumed positive when compressive, as indicated in Figure 12a.

Figure 12b represents the so called ground reaction curve of the borehole. The vertical axis represents the ratio of internal pressure and far-field stress, while the horizontal axis represents a scaled measure of the radial displacement at the borehole wall. The scaling chosen for the horizontal axis is such that if the rock remains elastic after the internal pressure has been removed, the resulting value is one (see the intersection point of the extension of the line labelled as 'Elastic' and the horizontal axis in Figure 12b). In general, the ground reaction curve represented in Figure 12b has an elastic and a plastic part. Point P_0 corresponds to the initial condition for which internal pressure and far-field stresses are equal, and therefore, no radial displacement takes place. Point P_1 corresponds an intermediate condition for which the internal pressure is equal to the critical internal pressure (p_i^{cr}) and the plastic region starts to the develop around the hole. Point P_3 corresponds to the final condition in which the internal pressure has been removed and the radial displacement at the wall has reached the maximum and final value.

Figure 13 is a combined representation of the ground reaction curve discussed above, together with the graphical representation of the extent of the plastic region, R_{pl}/R —notice that R_{pl}/R is read on the vertical axis on the right of the diagram. Point P_1' is associated with the point P_1 in the ground reaction curve, and therefore corresponds to the condition when the plastic region is starting to develop (i.e., $R_{pl}/R = 1$). Point P_2' is associated with the point P_2 in the ground reaction curve, and therefore corresponds to final condition in which the internal pressure has been removed and the extent of the plastic region reaches its final value.

In the following sections the equations conforming the full elasto-plastic solution of the problem in Figure 12a are provided.

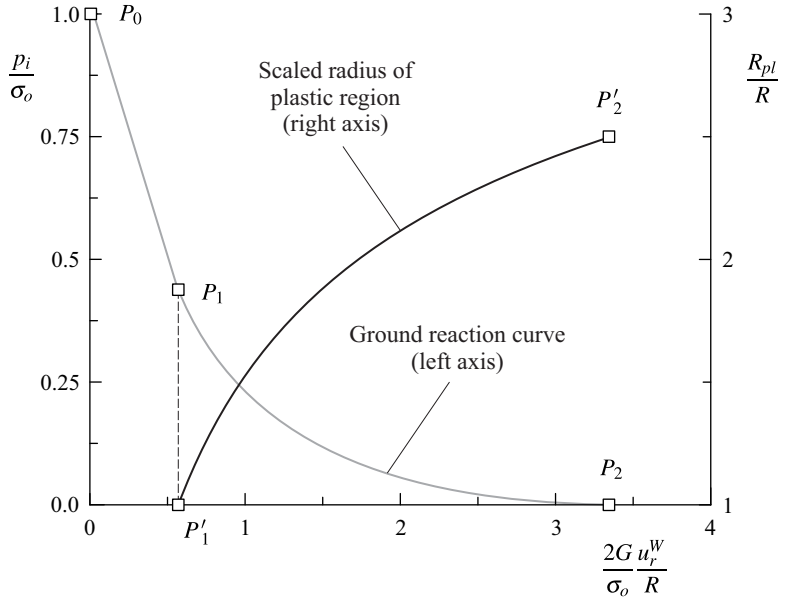

Figure 13. Ground reaction curve and extent of plastic region presentations for the problem in Figure 12a.

5.2. Elastic solution

If the internal pressure is larger than the critical internal pressure (i.e., if $p_i > p_i^{cr}$), the rock remains elastic and the solution for the radial stress, $\sigma_r(r)$, hoop stress, $\sigma_\theta(r)$, and radial displacement, $u_r(r)$, is given by the following equations (see, for example, Davis & Selvadurai 1996; Jaeger et al. 2007)

$$\sigma_r(r) = \sigma_o - (\sigma_o - p_i)\left(\frac{R}{r}\right)^2 \tag{77}$$

$$\sigma_\theta(r) = \sigma_o + (\sigma_o - p_i)\left(\frac{R}{r}\right)^2 \tag{78}$$

$$u_r(r) = \frac{1}{2G}(\sigma_o - p_i)\frac{R^2}{r} \tag{79}$$

If the critical internal pressure is negative (i.e., tension needs to be applied to the borehole wall to reach the critical pressure), then the internal pressure can be decreased to zero and the material will remain elastic; in that case, the radial displacement of the borehole wall is obtained making $p_i = 0$ and $r = R$ in equation (79); this gives

$$u_r^W = \frac{R}{2G}\sigma_o \tag{80}$$

If the internal pressure is smaller than the critical internal pressure (i.e., if $p_i < p_i^{cr}$), the rock around the borehole becomes plastic and the extent of plastic failure, distribution of radial and hoop stresses, and radial displacements depend on the failure criterion being considered.

Appendix C presents the general elasto-plastic formulation for the general scaled power law failure criterion

introduced in Section 3.1. The following three sections provide the elasto-plastic solution for rocks that obey the Mohr-Coulomb, Hoek-Brown and Fairhurst failure criteria, respectively.

5.3. Dimensionless solution for scaled Mohr-Coulomb intact rock

Stresses are scaled using the rule that applies to the Mohr-Coulomb failure criterion in Section 3.2 (capital 'S' denotes scaled stresses). The scaled far-field stresses, internal pressure and critical internal pressure are as follows,

$$S_o = \frac{\sigma_o}{\sigma_c} + \frac{1}{r_i} \qquad P_i = \frac{p_i}{\sigma_c} + \frac{1}{r_i} \qquad \text{and} \qquad P_i^{cr} = \frac{p_i^{cr}}{\sigma_c} + \frac{1}{r_i} \tag{81}$$

In equations (81), and in all equations that follow, σ_c is the unconfined compression strength of the rock and r_i is the ratio of unconfined compression strength and biaxial tensile strength given by equation (17).

Radial and hoop stresses are also scaled as follows

$$S_r(r) = \frac{\sigma_r(r)}{\sigma_c} + \frac{1}{r_i} \qquad \text{and} \qquad S_\theta(r) = \frac{\sigma_\theta(r)}{\sigma_c} + \frac{1}{r_i} \tag{82}$$

The equations that follow result from application of the procedure outlined in Appendix C. For the case of Mohr-Coulomb material, the differential equations (C-11) through (C-13) in Appendix C can be solved exactly, and closed-form equations for all field functions can be obtained.

The scaled critical internal pressure is

$$P_i^{cr} = \frac{2S_o}{r_i + 2} \tag{83}$$

while the extent of the plastic region is

$$\frac{R_{pl}}{R} = \left(\frac{P_i^{cr}}{P_i}\right)^{\frac{1}{r_i}} \tag{84}$$

The solution for the scaled radial stress, $S_r(r)$, scaled hoop stress, $S_\theta(r)$, and radial displacement, $u_r(r)$, for the plastic region ($r \le R_{pl}$ in Figure 12a) is

$$S_r(r) = P_i^{cr}\left(\frac{r}{R_{pl}}\right)^{r_i} \tag{85}$$

$$S_\theta(r) = (r_i + 1)\, P_i^{cr}\left(\frac{r}{R_{pl}}\right)^{r_i} \tag{86}$$

$$\begin{aligned}\frac{2G}{\sigma_c}\frac{u_r(r)}{R_{pl}} = {} & \frac{r_i}{2(1-A_1)}\left[2\left(\frac{r}{R_{pl}}\right)^{A_1} - (1+A_1)\frac{r}{R_{pl}}\right] P_i^{cr} \\ & - \frac{A_2 - A_3(r_i+1)}{(1-A_1)(r_i+1-A_1)}\left[(r_i+1-A_1)\frac{r}{R_{pl}} - r_i\left(\frac{r}{R_{pl}}\right)^{A_1} - (1-A_1)\left(\frac{r}{R_{pl}}\right)^{r_i+1}\right] P_i^{cr}\end{aligned} \tag{87}$$

where

$$A_1 = -K_\psi \qquad A_2 = 1 - \nu(1+K_\psi) \qquad A_3 = \nu - (1-\nu)K_\psi \tag{88}$$

and

$$K_\psi = \frac{1+\sin\psi}{1-\sin\psi} \tag{89}$$

The radial displacement of the borehole wall, u_r^W, is obtained from equation (87), making $r = R$, thus

$$\frac{2G}{\sigma_c}\frac{u_r^W}{R_{pl}} = \frac{2G}{\sigma_c}\frac{u_r(R)}{R_{pl}} \tag{90}$$

The solution for $S_r(r)$, $S_\theta(r)$, and $u_r(r)$, for the elastic region ($r \geq R_{pl}$ in Figure 12a) is

$$S_r(r) = S_o - (S_o - P_i^{cr})\left(\frac{R_{pl}}{r}\right)^2 \tag{91}$$

$$S_\theta(r) = S_o + (S_o - P_i^{cr})\left(\frac{R_{pl}}{r}\right)^2 \tag{92}$$

$$\frac{2G}{\sigma_c}\frac{u_r(r)}{R_{pl}} = (S_o - P_i^{cr})\frac{R_{pl}}{r} \tag{93}$$

The elasto-pastic solution conformed by equations (83) through (93) is the same solution presented in Carranza-Torres (2002; 2003).

A scaled version of the ground reaction curve in Figures 12b and 13 can be constructed plotting the ratio P_i/S_o defined by the first two equations (81) in the vertical axis, and the ratio $u_r^W/R\ 2\tilde{G}/S_o$ defined by equation (90) (see also equation C-7) in the horizontal axis. In such plot, different curves correspond to different ratios r_i. In addition, a dimensionless graphical representation of the scaled extent of the plastic region similar to that in Figure 13 can be constructed plotting the ratio R_{pl}/R defined by equation (84) in the vertical axis, and the same scaled radial displacement as for the mentioned ground reaction curve. These dimensionless diagrams, that are included in Figure 14, conform what they can be called *global* representations of the ground reaction curve (and extent of plastic region) for a borehole in a rock that satisfies the Mohr-Coulomb failure criterion. This is because every possible ground reaction curve (and plastic extent curve) for boreholes in Mohr-Coulomb rock can be constructed based on these dimensionless representations.

As an example, the points labelled as P with superscripts A, B and C in Figure 14 correspond to the same points P in Figure 13, for the cases designated as Cases A, B and C in Table 4. Although all three cases have different values of the variables σ_o and σ_c, they all have the same ratio r_i. Cases C, B and A (in that order) correspond to boreholes in different rocks that have decreasing values of unconfined compression strength, σ_c, relative to the far-field stresses σ_o acting on the rock —see Table 4. Therefore the wall displacements and extents of plastic failure are progressively larger (for the same scaled internal pressure) for Cases C, B and A (in that order). This can be readily seen in the diagrams of Figure 15, which corresponds to the actual ground reaction curves and extent of plastic failure diagrams in terms of unscaled stresses, for the three mentioned cases, constructed from the global representations in Figure 14.

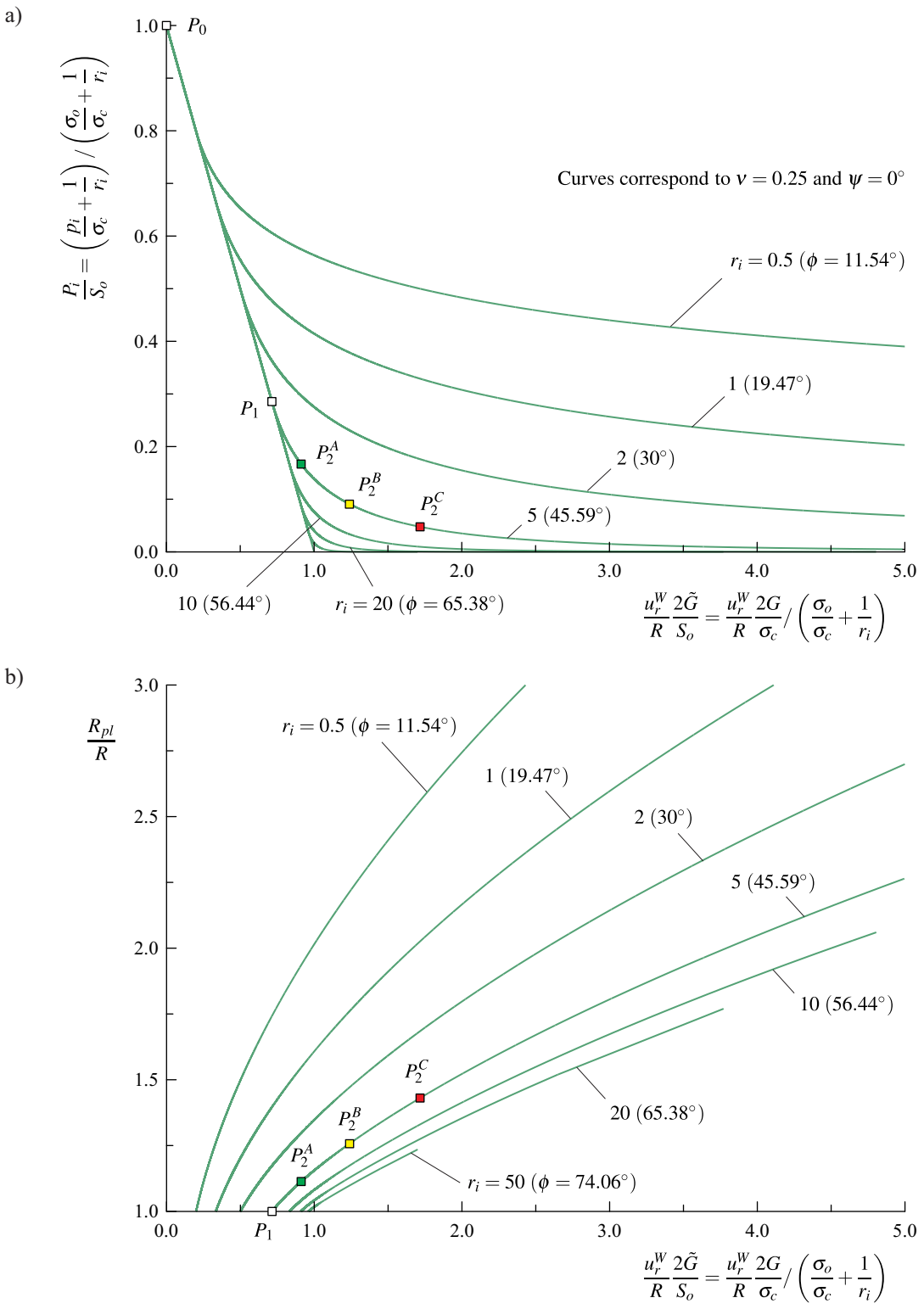

Figure 14. Global a) ground reaction curve and b) extent of plastic region representations for a borehole driven in rock that satisfies the Mohr-Coulomb failure criterion.

Table 4. Cases of boreholes driven in rocks that satisfy the Mohr-Coulomb failure criterion, represented in Figure 14.

Data

Case	σ_o [MPa]	σ_c [MPa]	r_i [-]	ϕ [°]	G [GPa]
A	50	50	5	45.6	25
B	80	40	5	45.6	16
C	40	10	5	45.6	3

Note: All three cases assume $\nu = 0.25$ and $\psi = 0°$.

Results. Actual stresses

Case	p_i^{cr}/σ_o [-]	p_i/σ_o [-]	R_{pl}/R [-]	u_r^W/R [%]
A	0.143	0.00	1.114	0.110
B	0.214	0.00	1.257	0.341
C	0.250	0.00	1.431	1.202

Results. Scaled stresses

Case	P_i^{cr}/S_o [-]	P_i/S_o [-]	R_{pl}/R [-]	$u_r^W/R\ 2\tilde{G}/S_o$ [-]
A	0.286	0.167	1.114	0.913
B	0.286	0.091	1.257	1.239
C	0.286	0.048	1.431	1.718

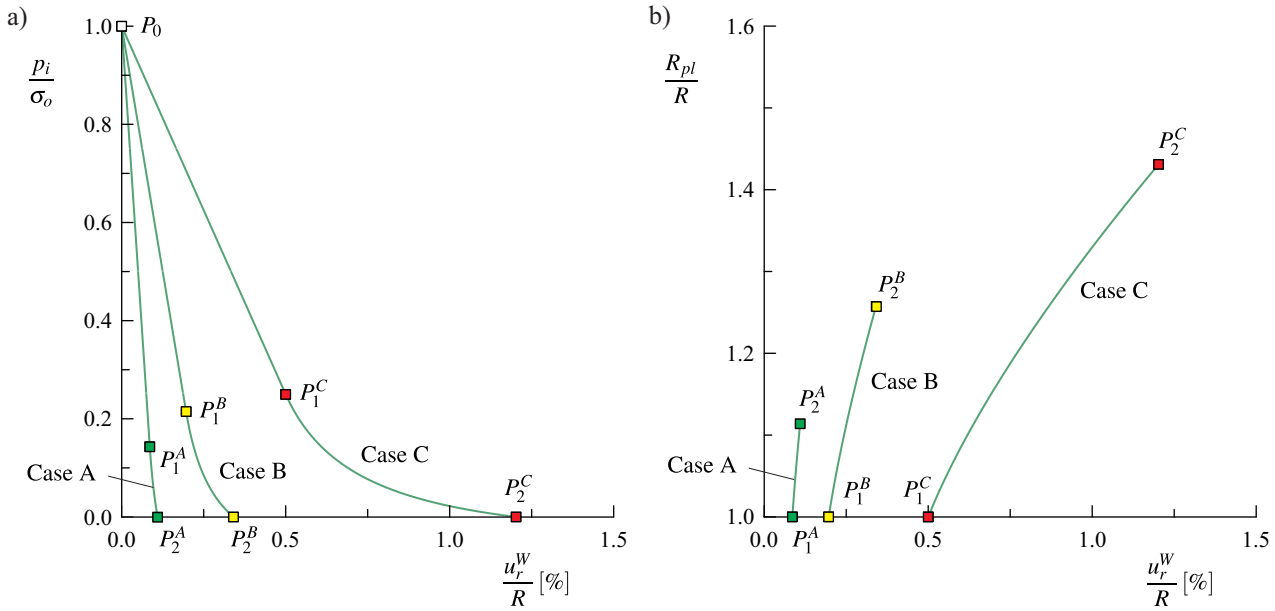

Figure 15. a) Ground reaction curve and b) extent of plastic region representations for three cases of borehole driven in rocks that satisfy the Mohr-Coulomb failure criterion, constructed from the global representations in Figure 14.

5.4. Dimensionless solution for scaled Hoek-Brown intact rock

Stresses are scaled using the rule that applies to the Hoek-Brown failure criterion in Section 3.3 (capital 'S' denotes scaled stresses). The scaled far-field stresses, internal pressure and critical internal pressure are as follows,

$$S_o = \left(\frac{\sigma_o}{\sigma_c} + \frac{1}{m_i}\right)\frac{1}{m_i} \qquad P_i = \left(\frac{p_i}{\sigma_c} + \frac{1}{m_i}\right)\frac{1}{m_i} \qquad \text{and} \qquad P_i^{cr} = \left(\frac{p_i^{cr}}{\sigma_c} + \frac{1}{m_i}\right)\frac{1}{m_i} \tag{94}$$

In equations (94), σ_c is the unconfined compression strength of the rock and m_i is the ratio of unconfined compression strength and biaxial tensile strength given by equation (31).

Radial and hoop stresses are also scaled as follows

$$S_r(r) = \left[\frac{\sigma_r(r)}{\sigma_c} + \frac{1}{m_i}\right]\frac{1}{m_i} \qquad \text{and} \qquad S_\theta(r) = \left[\frac{\sigma_\theta(r)}{\sigma_c} + \frac{1}{m_i}\right]\frac{1}{m_i} \tag{95}$$

The equations that follow result from application of the procedure outlined in Appendix C. For the case of Hoek-Brown material, the differential equations (C-11) through (C-13) in Appendix C can be solved exactly, and closed-form equations for all field functions can be obtained.

The scaled critical internal pressure is

$$P_i^{cr} = \frac{1}{16}\left(1 - \sqrt{16S_o + 1}\right)^2 \tag{96}$$

while the extent of the plastic region is

$$\frac{R_{pl}}{R} = \exp\left[2\left(\sqrt{P_i^{cr}} - \sqrt{P_i}\right)\right] \tag{97}$$

The solution for the scaled radial stress, $S_r(r)$, scaled hoop stress, $S_\theta(r)$, and radial displacement, $u_r(r)$, for the plastic region ($r \le R_{pl}$ in Figure 12a) is

$$S_r(r) = \left[\sqrt{P_i^{cr}} + \frac{1}{2}\ln\left(\frac{r}{R_{pl}}\right)\right]^2 \tag{98}$$

$$S_\theta(r) = S_r(r) + \sqrt{S_r(r)} \tag{99}$$

$$\begin{aligned}\frac{2G}{m_i\sigma_c}\frac{u_r(r)}{R_{pl}} = {} & \frac{K_\phi - 1}{2(1-A_1)}\left[2\left(\frac{r}{R_{pl}}\right)^{A_1} - (1+A_1)\frac{r}{R_{pl}}\right]\sqrt{P_i^{cr}} \\ & + \frac{A_2 - A_3}{4(1-A_1)}\frac{r}{R_{pl}}\left[\ln\left(\frac{r}{R_{pl}}\right)\right]^2 \\ & + \left[\frac{A_2 - A_3}{(1-A_1)^2}\sqrt{P_i^{cr}} - \frac{A_2 - A_1A_3}{2(1-A_1)^3}\right]\left[\left(\frac{r}{R_{pl}}\right)^{A_1} - \frac{r}{R_{pl}} + (1-A_1)\frac{r}{R_{pl}}\ln\left(\frac{r}{R_{pl}}\right)\right]\end{aligned} \tag{100}$$

The constants A_1, A_2 and A_3 in equation (100) are defined by the same equations (88).

The radial displacement of the borehole wall, u_r^W, is obtained from equation (100), making $r = R$, thus

$$\frac{2G}{m_i \sigma_c} \frac{u_r^W}{R_{pl}} = \frac{2G}{m_i \sigma_c} \frac{u_r(R)}{R_{pl}} \tag{101}$$

The solution for $S_r(r)$, $S_\theta(r)$, and $u_r(r)$, for the elastic region ($r \geq R_{pl}$ in Figure 12a) is given by the same equations (91) through (93).

The elasto-plastic solution conformed by equations (96) through (101) is the same solution presented in Carranza-Torres & Fairhurst (1999) and Carranza-Torres (2002).

A scaled version of the ground reaction curve in Figures 12b and 13 can be constructed plotting the ratio P_i/S_o defined by the first two equations (94) in the vertical axis, and the ratio $u_r^W/R\, 2\tilde{G}/S_o$ defined by equation (101) (see also equation C-8) in the horizontal axis. In such plot, different curves correspond to different scaled far-field stresses, S_o. In addition, a dimensionless graphical representation of the scaled extent of the plastic region similar to that in Figure 13 can be constructed plotting the ratio R_{pl}/R defined by equation (97) in the vertical axis, and the same scaled radial displacement as for the mentioned ground reaction curve. These dimensionless diagrams, that are included in Figure 16, conform *global* representations of the ground reaction curve (and extent of plastic region) for a borehole in a rock that satisfies the Hoek-Brown failure criterion. This is because every possible ground reaction curve (and plastic extent curve) for boreholes in Hoek-Brown rock can be constructed based on these dimensionless representations.

As an example, the points labelled as P with superscripts D, E and F in Figure 16 correspond to the same points P in Figure 13, for the cases designated as Cases D, E and F in Table 5. Although the cases correspond to different values of input variables σ_o, σ_c, m_i and G, all three cases have the same value of scaled far-field stress, S_o, equal to 0.5. Cases F, E and D (in that order) correspond to boreholes in different rocks that have decreasing values of unconfined compression strength, σ_c, relative to the far-field stresses σ_o acting on the rock —see Table 5. Therefore the wall displacements and extents of plastic failure are progressively larger (for the same scaled internal pressure) for Cases F, E and D (in that order). This can be readily seen in the diagrams of Figure 17, which correspond to the actual ground reaction curves and extent of plastic failure diagrams in terms of unscaled stresses, for the three mentioned cases, constructed from the global representations in Figure 16.

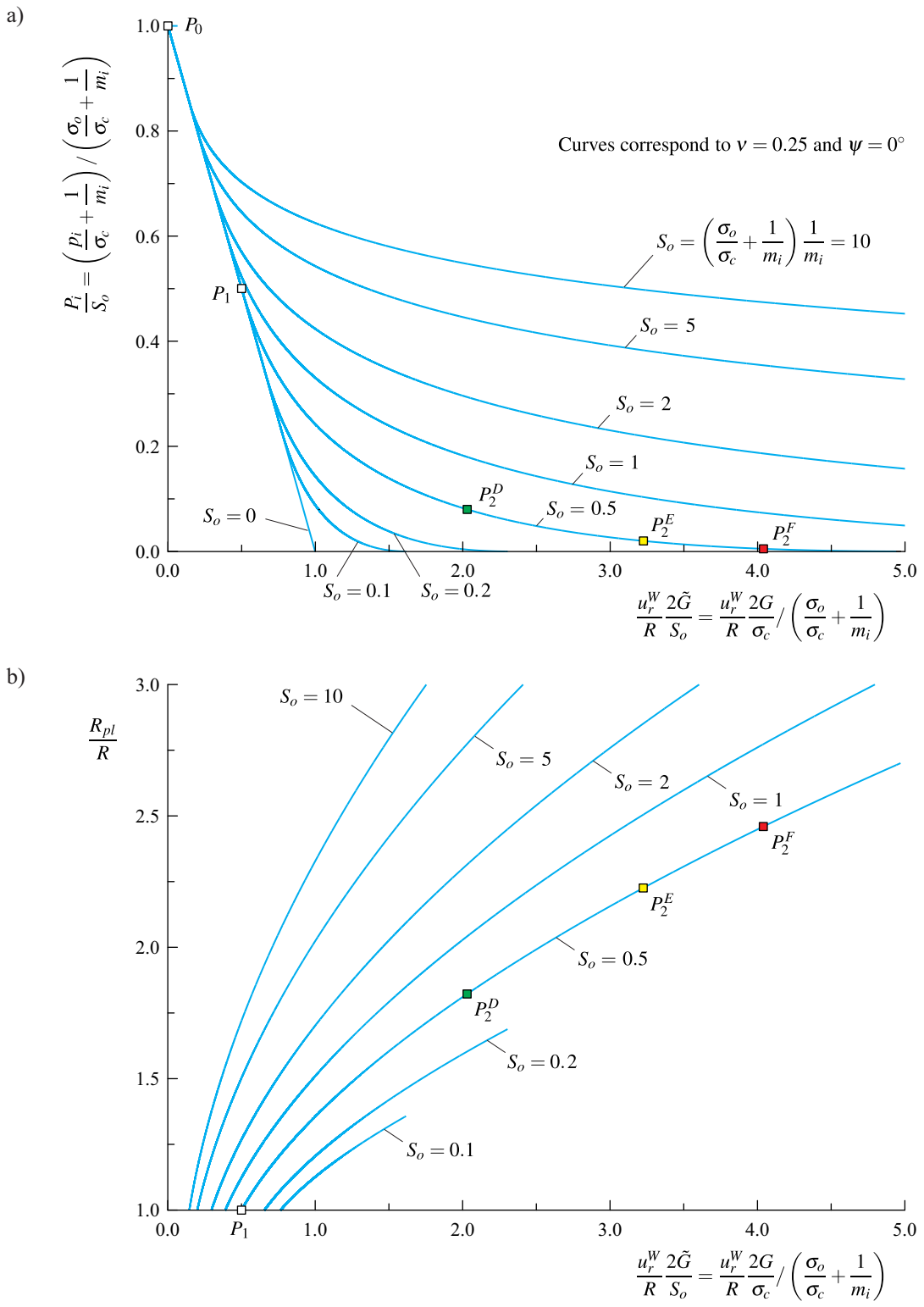

Figure 16. Global a) ground reaction curve and b) extent of plastic region representations for a borehole driven in rock that satisfies the Hoek-Brown failure criterion.

Table 5. Cases of boreholes driven in rocks that satisfy the Hoek-Brown failure criterion, represented in Figure 16.

Data

Case	σ_o [MPa]	σ_c [MPa]	m_i [-]	G [GPa]	S_o [-]
D	80	34.78	5	14.78	0.5
E	120	29.49	10	11.02	0.5
F	150	15.08	20	6.03	0.5

Note: All three cases assume $\nu = 0.25$ and $\psi = 0^\circ$.

Results. Actual stresses

Case	p_i^{cr}/σ_o [-]	p_i/σ_o [-]	R_{pl}/R [-]	u_r^W/R [%]
D	0.457	0.00	1.822	0.597
E	0.490	0.00	2.226	1.792
F	0.497	0.00	2.460	5.050

Results. Scaled stresses

Case	P_i^{cr}/S_o [-]	P_i/S_o [-]	R_{pl}/R [-]	$u_r^W/R\ 2\tilde{G}/S_o$ [-]
D	0.500	0.080	1.822	2.030
E	0.500	0.020	2.226	3.225
F	0.500	0.005	2.460	4.040

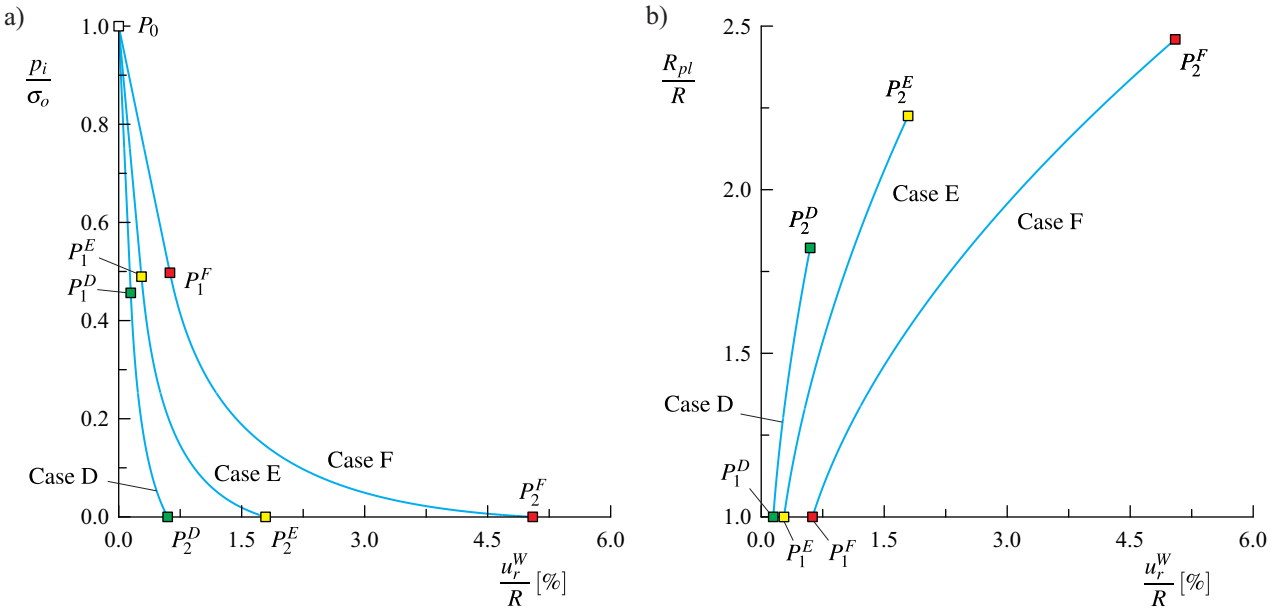

Figure 17. a) Ground reaction curve and b) extent of plastic region representations for three cases of borehole driven in rocks that satisfy the Hoek-Brown failure criterion, constructed from the global representations in Figure 16.

5.5. Dimensionless solution for scaled Fairhurst intact rock

Stresses are scaled using the rule that applies to the Fairhurst failure criterion in Section 3.4 (capital 'S' denotes scaled stresses). The scaled far-field stresses, internal pressure and critical internal pressure are as follows,

$$S_o = \left(\frac{\sigma_o}{\sigma_c} + \frac{1}{n_i}\right) \frac{n_i}{4\left(\sqrt{n_i+1}-1\right)^2} \qquad P_i = \left(\frac{p_i}{\sigma_c} + \frac{1}{n_i}\right) \frac{n_i}{4\left(\sqrt{n_i+1}-1\right)^2} \tag{102}$$

$$P_i^{cr} = \left(\frac{p_i^{cr}}{\sigma_c} + \frac{1}{n_i}\right) \frac{n_i}{4\left(\sqrt{n_i+1}-1\right)^2} \tag{103}$$

In equations (102) and (103), σ_c is the unconfined compression strength of the rock and n_i is the ratio of unconfined compression strength and biaxial tensile strength given by equation (40).

Radial and hoop stresses are also scaled as follows

$$S_r(r) = \left[\frac{\sigma_r(r)}{\sigma_c} + \frac{1}{n_i}\right] \frac{n_i}{4\left(\sqrt{n_i+1}-1\right)^2} \qquad \text{and} \qquad S_\theta(r) = \left[\frac{\sigma_\theta(r)}{\sigma_c} + \frac{1}{n_i}\right] \frac{n_i}{4\left(\sqrt{n_i+1}-1\right)^2} \tag{104}$$

The equations that follow result from application of the procedure outlined in Appendix C, that allows the elasto-plastic solution of the borehole problem for the Fairhurst failure criterion to be obtained. For the case of Fairhurst material, the differential equations (C-11) through (C-13) in Appendix C cannot be solved exactly, and closed-form equations for field functions are not possible. With the exception of the scaled critical internal pressure and scaled hoop stress for which a closed-form solution is possible, the other quantities require numerical integration. In the equations that follow, numerical integration is implied with the notation $f(x1, x2, ...)$ on the right side of the equation. The Fourth-order Runge-Kutta method may be used as a method of integration of the differential equations in Appendix C (see, for example, Press et al. 2007).

The scaled critical internal pressure is

$$P_i^{cr} = \frac{1}{16}\left(1 - \sqrt{16S_o - 1}\right)^2 \tag{105}$$

while the extent of the plastic region is

$$\frac{R_{pl}}{R} = f_1(P_i^{cr}, P_i) \tag{106}$$

The solution for the scaled radial stress, $S_r(r)$, scaled hoop stress, $S_\theta(r)$, and radial displacement, $u_r(r)$, for the plastic region ($r \le R_{pl}$ in Figure 12a) is

$$S_r(r) = f_2\left(P_i^{cr}, \frac{r}{R_{pl}}\right) \tag{107}$$

$$S_\theta(r) = S_r(r) + \sqrt{S_r(r)} + \frac{1}{4} \tag{108}$$

$$\frac{u_r(r)}{R_{pl}} = \frac{\sigma_c}{2G} \frac{4\left(\sqrt{n_i+1}-1\right)^2}{n_i} f_3\left(P_i^{cr}, \frac{r}{R_{pl}}, A_1, A_2, A_3\right) \tag{109}$$

The constants A_1, A_2 and A_3 in equation (109) are defined by the same equations (88).

The radial displacement of the borehole wall, u_r^W, is obtained from equation (109), making $r = R$, thus

$$\frac{u_r^W}{R_{pl}} = \frac{u_r(R)}{R_{pl}} \tag{110}$$

As discussed in Section 3.4, the Griffith failure criterion is recovered from the Fairhurst failure criterion when $n_i = 8$. Therefore equations (102) through (110) with $n_i = 8$ corresponds to the solution of a borehole in Griffith rock.

As in the case of boreholes in Mohr-Coulomb and Hoek-Brown rock discussed in Sections 5.3 and 5.4, respectively, a scaled version of the ground reaction curve in Figures 12b and 13 can be constructed plotting the ratio P_i/S_o defined by equations (102) in the vertical axis, and the ratio $u_r^W/R\ 2\tilde{G}/S_o$ defined by equation (110) (see also equation C-9) in the horizontal axis. In such plot, and as in the case of the borehole in Hoek-Brown rock discussed in Section 5.4, different curves correspond to different scaled far-field stresses, S_o. In addition, a dimensionless graphical representation of the scaled extent of the plastic region similar to that in Figure 13 can be constructed plotting the ratio R_{pl}/R given by equation (106) in the vertical axis, and the same scaled radial displacement as for the ground reaction curve. These dimensionless diagrams, that are included in Figure 18, conform *global* representations of the ground reaction curve (and extent of plastic region) for a borehole in a rock that satisfies the Fairhurst failure criterion. This is because every possible ground reaction curve (and plastic extent curve) for boreholes in Fairhurst rock can be constructed based on these dimensionless representations.

As an example, the points labelled as P with superscript D' in Figure 18 correspond to the same points P in Figure 13, for the case designated as Case D$'$ in Table 6. This case is the same Case D corresponding to Hoek-Brown parameter $m_i = 5$ in Table 5, but considering the Fairhurst parameter $n_i = 5$ (compare the row for Case D in the *Data* section of Table 5, with the row for Case D$'$ in the corresponding section of Table 6).

Figure 19a represents the same borehole problem in Figure 12a, considering that the rock obeys the Hoek-Brown failure criterion and the Fairhurst criterion, according to the properties listed for Cases D and D$'$ in Tables 5 and 6, respectively. Figure 19b shows the corresponding failure envelopes in a principal stress diagram. For a confined stress regime that is purely compressive (as it is the case of the borehole problem considered here), the shear strength predicted by Hoek-Brown failure criterion will be higher than that predicted by the Fairhurst failure criterion for the same value of the constants m_i and n_i, respectively. Since the Fairhurst failure criterion is based on the Griffith failure criterion, it can be argued that this failure criterion allows the extent of fracturing to be quantified. In this way, and referring to Figure 19, the Hoek-Brown failure criterion may be used to quantify the extent of failure, while the Fairhurst criterion may be used to quantify the extent of fracturing.

Figure 20 represents the actual ground reaction curves and extent of plastic failure diagram in terms of unscaled stresses, obtained from the global representations in Figures 16 and 18. In view that the shear strength predicted by the Fairhurst failure criterion is smaller than that predicted by the Hoek-Brown failure criterion, the representations in Figure 20 shows larger displacements and larger extent of failure (for the same internal pressure) for the case of Fairhurst failure criterion compared with the Hoek-Brown failure criterion.

The Fairhurst constitutive model was written in the internal scripting language of the software FLAC (Itasca Consulting Group, Inc. 2016) and the borehole problem in Figure 19 was solved using the mesh of elements represented in Figure 21a, for zero internal pressure. The resulting distribution of radial and hoop stresses, and radial displacement is represented with dots in Figures 21b and 21c, respectively. As a reference, the

analytical solutions for both Fairhurst and Hoek-Brown failure criteria are represented with continuous lines. A good match is found between FLAC results and analytical results.

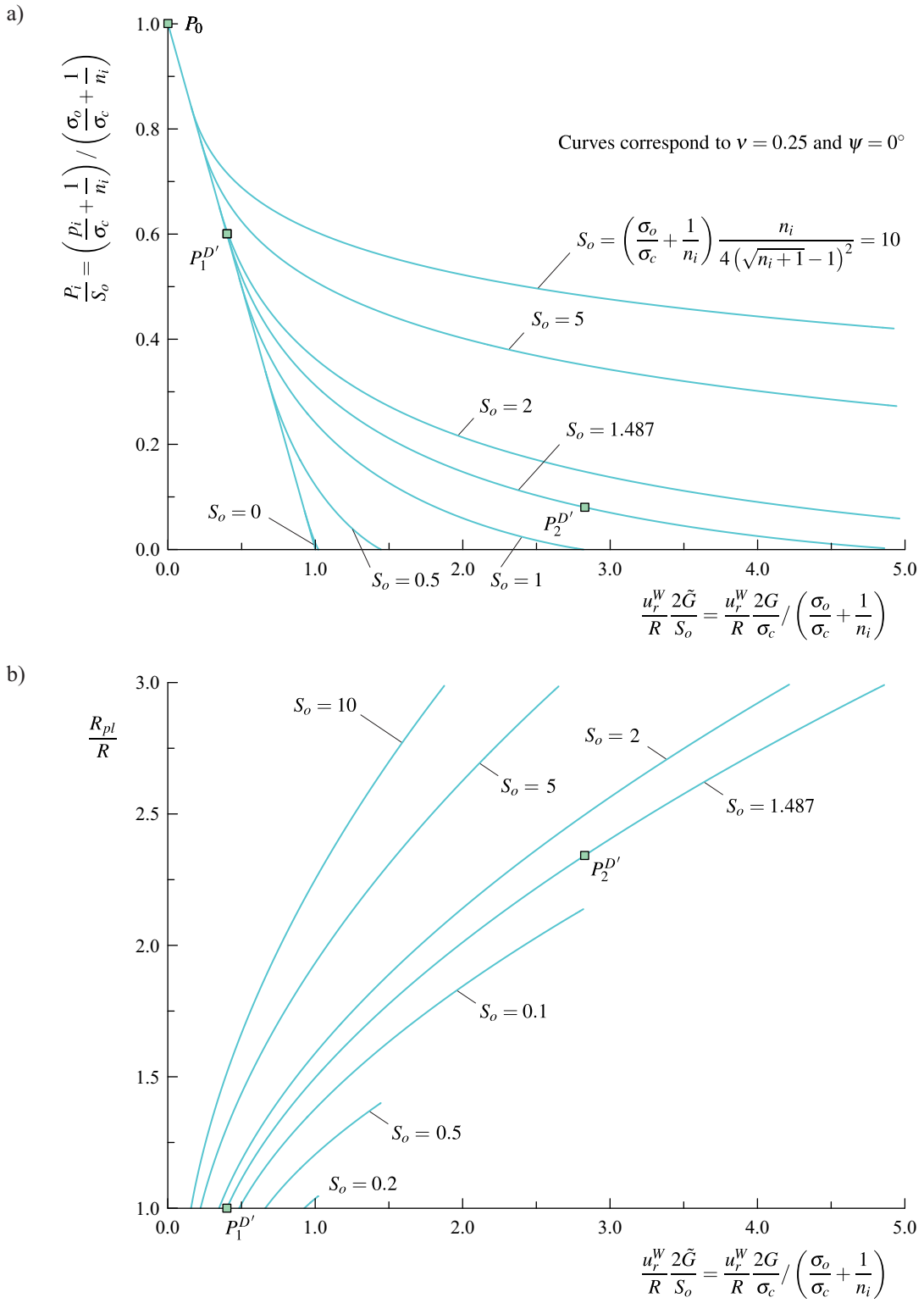

Figure 18. Global a) ground reaction curve and b) extent of plastic region representations for a borehole driven in rock that satisfies the Fairhurst failure criterion.

Table 6. Case of borehole driven in rock that satisfies the Fairhurst failure criterion, represented in Figure 18.

Data

Case	σ_o [MPa]	σ_c [MPa]	n_i [-]	G [GPa]	S_o [-]
D′	80	34.78	5	14.78	1.487

Note: The case assumes $\nu = 0.25$ and $\psi = 0°$.

Results. Actual stresses

Case	p_i^{cr}/σ_o [-]	p_i/σ_o [-]	R_{pl}/R [-]	u_r^W/R [%]
D′	0.564	0.00	2.338	0.832

Results. Scaled stresses

Case	P_i^{cr}/S_o [-]	P_i/S_o [-]	R_{pl}/R [-]	$u_r^W/R\ 2\tilde{G}/S_o$ [-]
D′	0.599	0.080	2.388	2.830

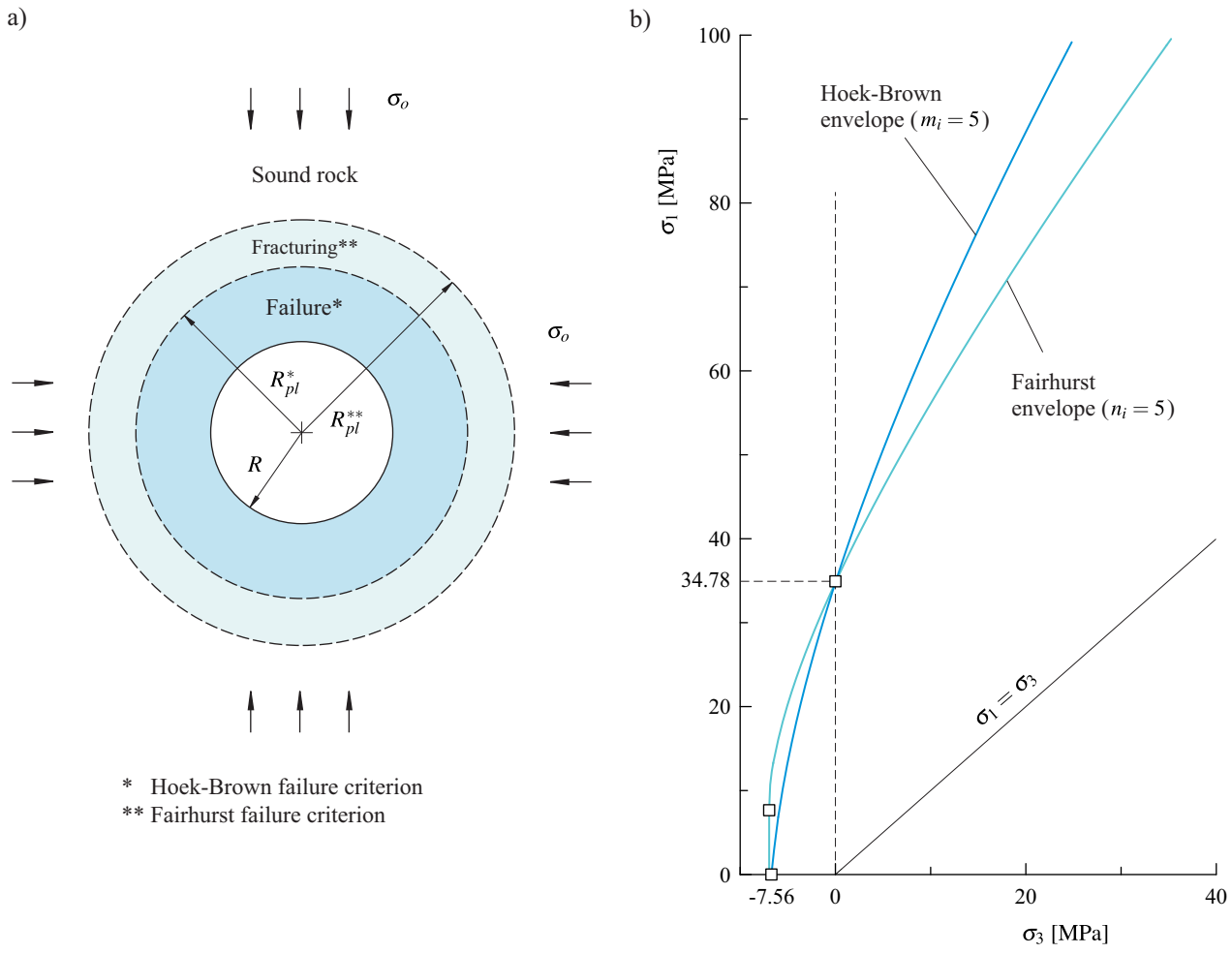

Figure 19. a) Borehole damage model considering failure region dictated by the Hoek-Brown failure criterion and fracturing region by the Fairhurst failure criterion. b) Failure envelopes corresponding to assumed ratios of compressive to tensile strength equal to 5, and unconfined compressive strength equal to 34.78 MPa.

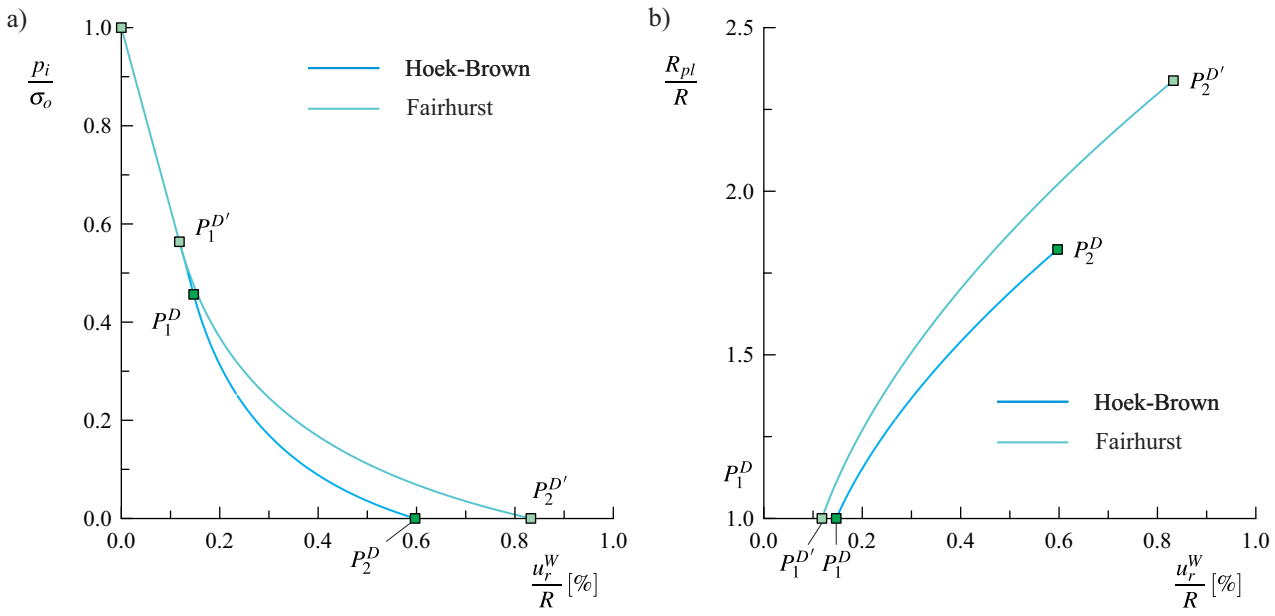

Figure 20. a) Ground reaction curve and b) extent of plastic region representations for borehole driven in rock that satisfies the Hoek-Brown and Fairhurst failure criteria, constructed from the global representations in Figures 16 and 18, respectively.

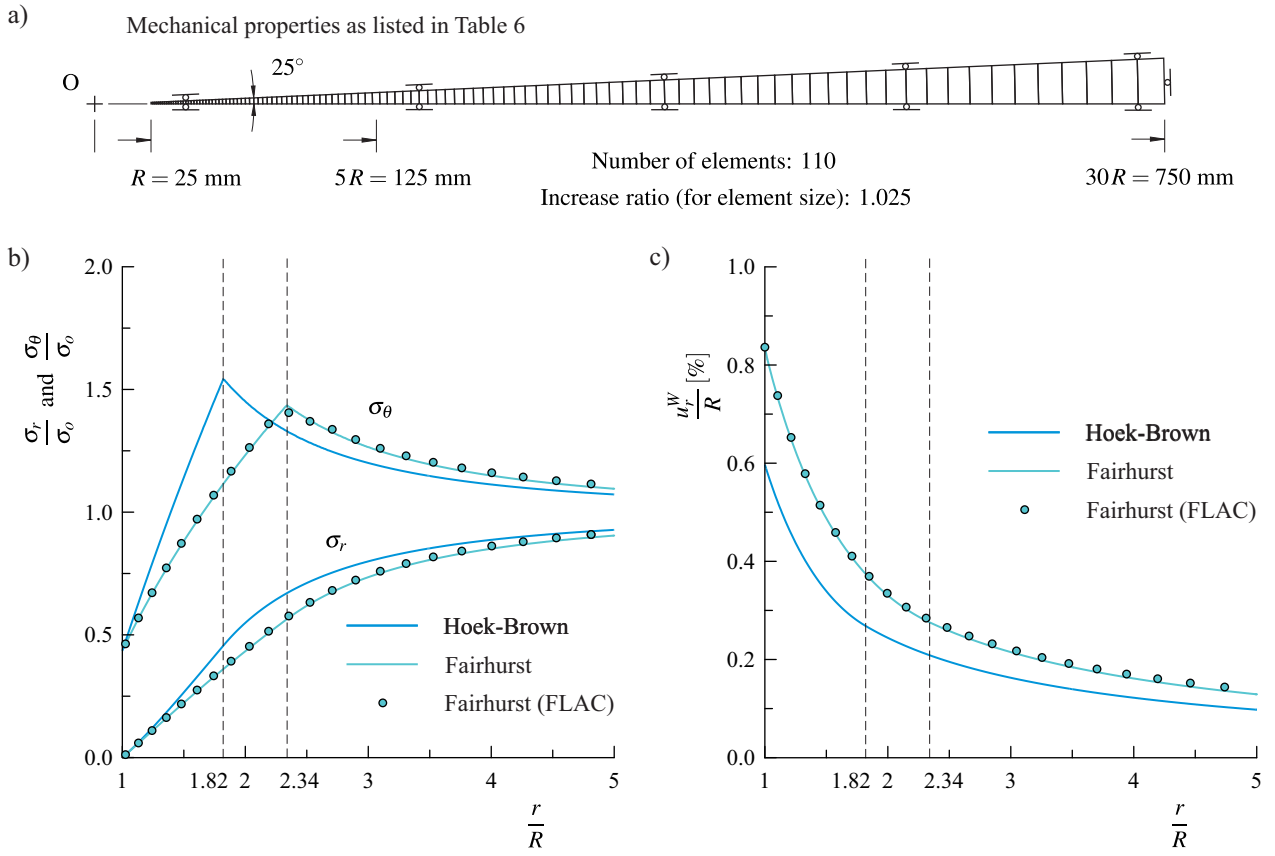

Figure 21. a) FLAC mesh used to model the axi-symmetric borehole problem in Figure 19, for a rock that obeys the Fairhurst failure criterion. b) Distribution of radial and hoop stresses, and c) distribution of radial displacements obtained with analytical and numerical solutions.

6. APPLICATION EXAMPLE 2: FACTOR OF SAFETY AND CRITICAL FAILURE SURFACE FOR AN UNCEMENTED ROCKFILL SLOPE

6.1. Problem statement

The second application example involves determining the factor of safety and the position of the assumed critical circular failure surface for a section of slope that results from dumping uncemented rockfill material that satisfies the Indraratna et al. failure criterion discussed in Section 4. Figure 22 is a schematic representation of the slope problem to be considered. The height of the slope is H and the angle of the slope is α. The bulk unit weight of the rockfill is γ and the shear strength of the rockfill is characterized by the parameters A, B and σ_{cF} introduced in Section 4. There is an infinitely strong horizontal surface at the base of the slope, which the critical failure surface is unable to cut through. The origin of a cartesian system of coordinates (x,y) is located at the toe of the slope. The center of the critical circular failure surface is at point P_c (of coordinates x_c and y_c), the starting point at the slope base is P_1 (of coordinates x_1 and y_1) and the exit point at the slope crest is P_3 (of coordinates x_3 and y_3). The critical failure surface may show a horizontal portion between the point P_1 and an intermediate point P_2 (of coordinates x_2 and y_2) at the base of the slope.

From dimensional analysis, the characteristic stress for the problem in Figure 22 is γH. When the scaling rule introduced in Section 4 is applied to this stress (see equations 74), it can be shown that the factor of safety, FS, is a function of dimensionless variables as follows

$$FS = f_{FS}\left(\frac{\gamma H}{\sigma_{cF}} A^{-1/(1-B)}, B, \alpha\right) \qquad \text{if} \qquad 0.5 \leq B < 1 \tag{111}$$

and

$$FS = f_{FS}\left(\frac{\gamma H}{\sigma_{cF}}, A, \alpha\right) \qquad \text{if} \qquad B = 1 \tag{112}$$

The solution of the problem for the case $B = 1$, corresponds to the solution of a slope in a Mohr-Coulomb cohesionless material. This problem as been discussed in many publications. In particular, an analysis similar to the one to be presented here is presented in Carranza-Torres & Hormazabal (2018).

The following section discusses the solution for the case $B \neq 1$, when the factor of safety is governed by equation (111).

6.2. Dimensionless solution

A large number of limit equilibrium SLIDE (Rocscience Inc. 2018) models were set up and computed to define the relationship between factor of safety and the dimensionless parameters given by equation (111). Six slope inclination angles corresponding to α equal to 20, 30, 40, 50, 60 and 70 degrees were considered. The approach used is that described in Carranza-Torres & Hormazabal (2018; 2020). Although other values of the rockfill parameter B were also evaluated, to illustrate the approach, the results presented here are for the case $B = 0.75$, which corresponds to the set of triaxial test results on large samples of rockfill discussed in Section 4.

Figure 23 represents graphically the relationship between the factor of safety and the dimensionless factor $\gamma H/\sigma_{cF} A^{-1/(1-B)}$ obtained for the different slope angles, and for the value $B = 0.75$. When plotted in logarithmic scale, the relationship resulted linear with all the lines corresponding to different slope angles being parallel to each other. The coordinates of the different points P in Figure 22 that characterize the

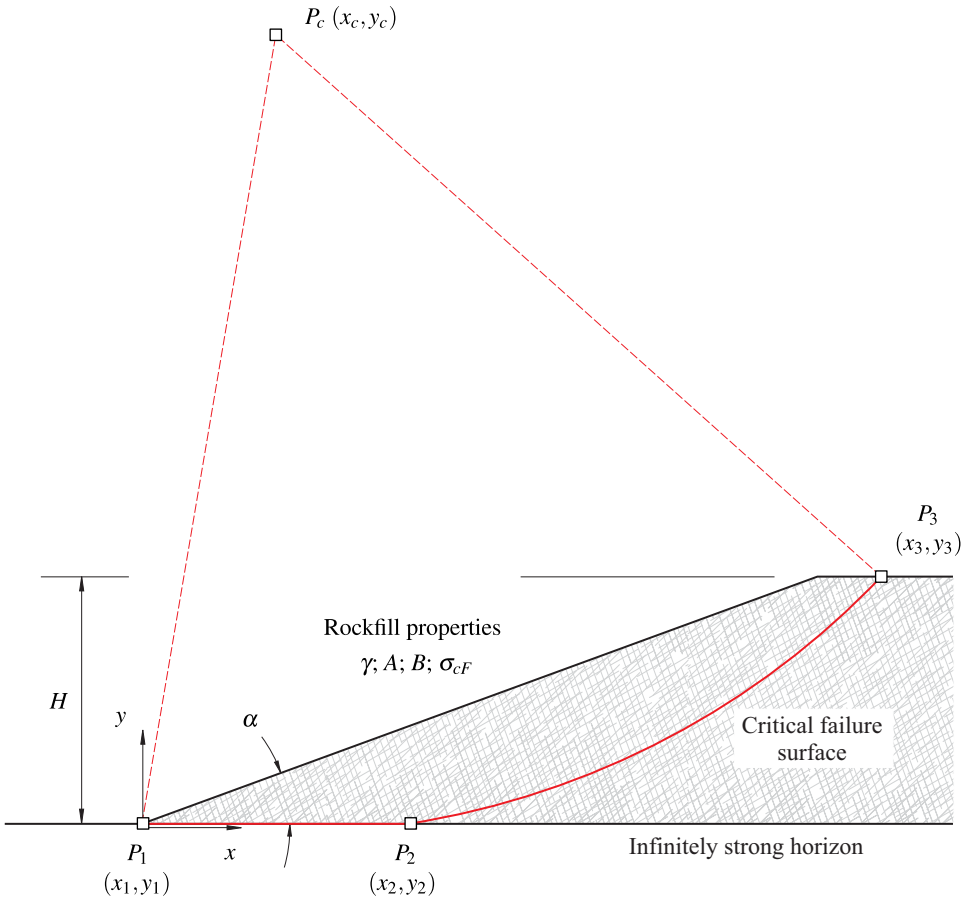

Figure 22. Problem of determining the factor of safety for a rockfill slope, assuming a critical *circular* failure surface.

critical circular failure surface, scaled with the height of the slope, resulted to be independent of the factor $\gamma H/\sigma_{cF} A^{-1/(1-B)}$ and to depend on the slope inclination angle only. The resulting scaled coordinates of the points P in Figure 22 are listed in Table 7 and these were used to construct the dimensionless slope sketches on the upper part of Figure 23. In the dimensionless diagram in Figure 23, the different points on the line corresponding to $\alpha = 40^\circ$ correspond to different slope cases to be discussed next. A regression analysis was done for the factor of safety results from the limit equilibrium models represented in Figure 23, and a closed-form equation for the factor of safety for slopes was obtained. The equation, which is valid when $B = 0.75$, is as follows

$$FS = \exp\left[\frac{54{,}027}{50{,}000} - \left(\frac{145{,}869}{50{,}000} \times 10^{-2}\right)\alpha + \left(\frac{95{,}433}{25{,}000} \times 10^{-4}\right)\alpha^2 - \left(\frac{127{,}411}{50{,}000} \times 10^{-6}\right)\alpha^3 - 0.25 \log\left(\frac{\gamma H}{\sigma_{cF}} A^{-4}\right)\right] \tag{113}$$

In equation (113), α is to be entered in degrees.

To illustrate the use of Figure 23 (and equation 113), a set of five initial cases, named Case 1, 2, 3, 4 and 5, are listed in Table 8. A second set of cases, named Cases 1a, 1b, 1c, 1d, 1e and 1f are listed in Table 9. All these cases are represented as the different points C (with subscripts indicating the case) in Figure 23.

Starting with the cases listed in Table 8, Cases 1, 2 and 3 correspond to slopes of same inclination angle, $\alpha = 40^\circ$, but different heights, H. In Table 8, the rockfill properties are denoted as A^*, B^* and σ^*_{cF} (notice

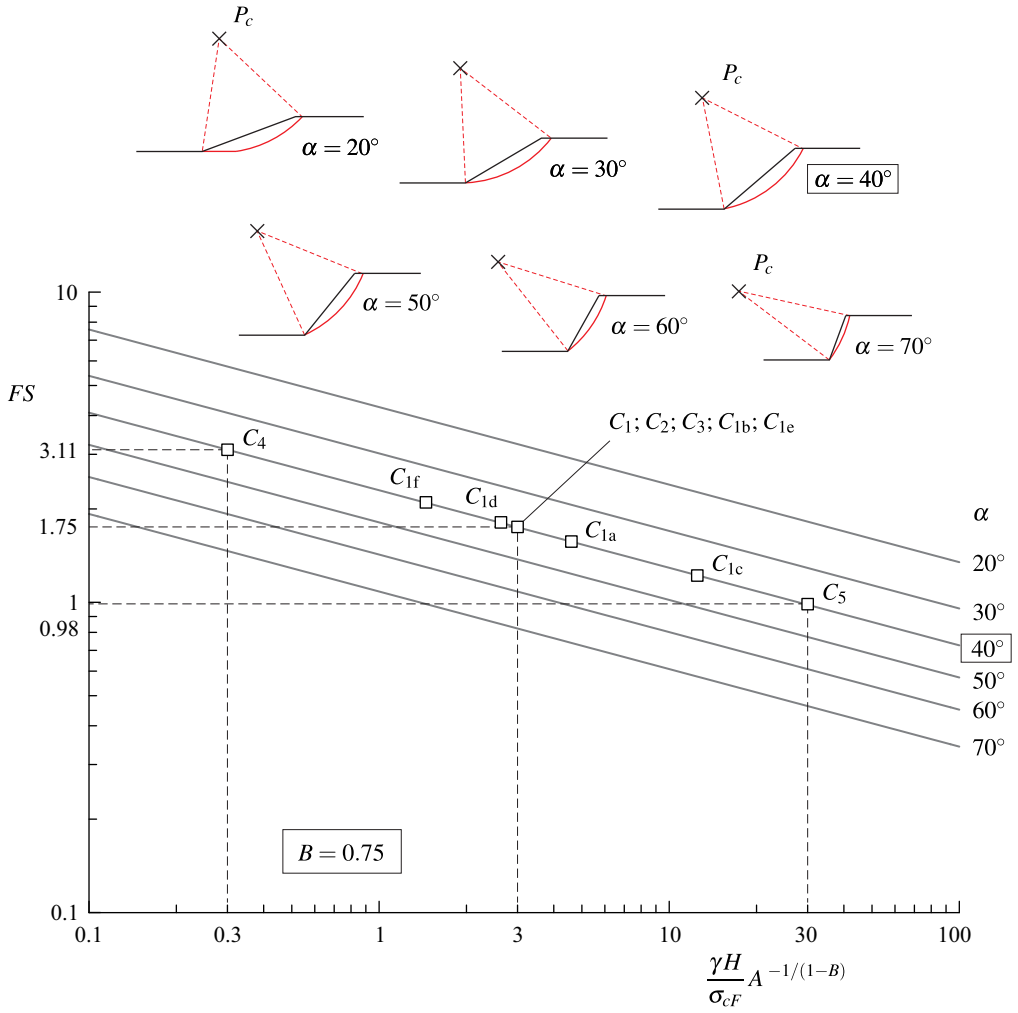

Figure 23. Dimensionless representation of factor of safety defined by limit equilibrium SLIDE models for the problem in Figure 22.

Table 7. Coordinates of points defining the critical circular failure surface in Figure 22, defined by limit equilibrium SLIDE models.

α [°]	x_c/H [-]	y_c/H [-]	x_1/H [-]	y_1/H [-]	x_2/H [-]	y_2/H [-]	x_3/H [-]	y_3/H [-]
20	0.55	3.20	0.00	0.00	1.10	0.00	2.94	1.00
30	-0.12	2.56	0.00	0.00	0.00	0.00	1.91	1.00
40	-0.35	1.83	0.00	0.00	0.00	0.00	1.32	1.00
50	-0.77	1.69	0.00	0.00	0.00	0.00	0.95	1.00
60	-1.28	1.61	0.00	0.00	0.00	0.00	0.68	1.00
70	-2.09	1.55	0.00	0.00	0.00	0.00	0.45	1.00

the use of an asterisk in the variable name) to imply, as explained in Section 4, that these are *measured* properties —the reason for doing this will become clear when discussing the cases in Table 9. In Table 8, the unit weight γ and the parameters A^* and σ^*_{cF} are different for all cases, but these values are such that all three cases have the same dimensionless factor $\gamma H/\sigma^*_{cF}\, A^{*-1/(1-B^*)}$ equal to 3. Cases 1, 2 and 3 plot as the same point labelled as C_1, C_2 and C_3 in Figure 23. The resulting factor of safety is 1.75 (see lower part of Table 8). Although the scaled coordinates of the points defining the critical circular failure surface are the same (see scaled coordinates for $\alpha = 40^\circ$ in Table 7), the actual coordinates are different, as indicated in the lower part of Table 8.

Cases 4 and 5 listed in Table 8 are comparable to Case 1, except that the height of the slope in Case 4 is 10 times smaller than the height of the reference Case 1. Similarly, the height of the slope in Case 5 is 10 times larger than that of Case 1 (the height of the slope for Case 5 is unrealistically large and is considered here for illustration purposes only). Considering that for Case 1 the dimensionless factor $\gamma H/\sigma^*_{cF}\, A^{*-1/(1-B^*)}$ is equal to 3, this dimensionless factor becomes 0.3 and 30 for Cases 4 and 5, respectively. Cases 4 and 5 plot as the points labelled as C_4 and C_5 in Figure 23. The resulting factors of safety for these cases are 3.11 and 0.98, respectively (see Figure 23 and lower part of Table 8). As expected, these are larger and smaller, respectively, than the factor of safety of 1.75 for the reference Case 1.

The different cases listed in Table 9 correspond to different variations of the Case 1 in Table 8. The purpose of including the additional cases in Table 9 is to show the effect of the unconfined compressive strength of the rockfill fragments, σ_{cF}, on the factor of safety, and to illustrate the use of the equations (68) through (72) in Section 4.

The first row in Table 9 corresponds to Case 1 (this has been transcribed from Table 8). Cases 1a, 1b and 1c in Table 9 correspond to cases for which the value of unconfined compressive strength of the rockfill (σ_{cF}) is smaller than for Case 1 (i.e., smaller than the value $\sigma^*_{cF} = 122.52$ MPa measured with the properties A^* and B^* in Table 9), and equal to 80 MPa. Cases 1d, 1e and 1f correspond to values of σ_{cF} larger than for Case 1, and equal to 140 MPa.

Cases 1a and 1d in Table 9, with the mentioned values of σ_{cF}, consider that the values of A and A^* are the same. Therefore, the shear strength ratio, $r_{\tau s}$, computed with equation (71) results to be 0.9 and 1.03, respectively. According to Figure 9, the shear strength for Case 1a can be expected to be smaller than the one for Case 1 (see point C_{1a} in Figure 9 —the abscissa of the point is 0.653 and it corresponds to the ratio $\sigma_{cF}/\sigma^*_{cF}$ equal to $80/122.52$), and the shear strength for Case 1d can be expected to be larger than the one for Case 1 (see point C_{1d} in Figure 9 —the abscissa of the point is 1.143 and it corresponds to the ratio $\sigma_{cF}/\sigma^*_{cF}$ equal to $140/122.52$). Consequently, for the rockfill slope problem of Figure 22, the factor of safety for Case 1a results smaller than that for Case 1 ($1.57 < 1.75$), and the factor of safety for Case 1d results larger than that for Case 1 ($1.81 > 1.75$).

Cases 1b and 1e in Table 9, assume that the shear strength ratio $r_{\tau s}$ given by equation (71) are both equal to 1.0 —this implies that the shear strength of the rockfill for Cases 1b and 1e are the same as for Case 1. Then, making $r_{\tau s} = 1$ in equation (72), the values of the parameter A for Cases 1b and 1e result to be 0.30 and 0.26, respectively. Since by making $r_{\tau s} = 1$ the values of σ_{cF} are prescribed not to have an effect on the strength of the rockfill, the factors of safety for Cases 1b and 1e are both equal to the factor of safety of Case 1 (i.e., they are all equal to 1.75).

Cases 1c and 1f in Table 9, assume that the shear strength ratios, $r_{\tau s}$, take arbitrarily selected values equal to 0.7 and 1.2 respectively. The corresponding values of the parameter A can be computed with equation (72), and these are listed in the corresponding rows in Table 9. Since the arbitrary values of $r_{\tau s}$ for Cases 1c and 1f lead to smaller and larger values than the values of the ratio for Cases 1a and 1d, respectively, the

Table 8. First set of cases of rockfill slopes represented in Figure 23.

Data

Case	γ [kN/m^3]	H [m]	σ^*_{cF} [MPa]	A^* [-]	$\frac{\gamma H}{\sigma^*_{cF}} A^{*\,-1/(1-B^*)}$ [-]
1	27.45	71.16	122.52	0.27	3
2	25.68	10.28	173.82	0.15	3
3	26.15	201.16	42.76	0.45	3
4	27.45	7.12	122.52	0.27	0.3
5	27.45	711.60	122.52	0.27	30

Note: All cases correspond to a slope angle $\alpha = 40^\circ$ and $B^* = 0.75$.

Results

Case	FS [-]	x_c [-]	y_c [-]	$x_1; x_2$ [-]	$y_1; y_2$ [-]	x_3 [-]	y_3 [-]
1	1.75	-24.91	130.22	0.00	0.00	93.93	71.16
2	1.75	-3.60	18.81	0.00	0.00	13.57	10.28
3	1.75	-70.41	368.12	0.00	0.00	265.53	201.16
4	3.11	-2.49	13.03	0.00	0.00	9.40	7.12
5	0.98	-249.06	1302.23	0.00	0.00	939.31	711.60

Table 9. Second set of cases of rockfill slopes represented in Figure 23.

Data

Case	γ [kN/m^3]	H [m]	σ^*_{cF} [MPa]	A^* [-]	σ_{cF} [MPa]	$r_{\tau s}$ [-]	A [-]	$\frac{\gamma H}{\sigma^*_{cF}} A^{*\,-1/(1-B^*)}$ [-]	$\frac{\gamma H}{\sigma_{cF}} A^{-1/(1-B)}$ [-]
1	27.45	71.16	122.52	0.27	122.52	1.0	0.27	3	3
1a	27.45	71.16	122.52	0.27	80	0.9 *	0.27	3	4.6
1b						1.0 **	0.30		3
1c						0.7 **	0.21		12.5
1d	27.45	71.16	122.52	0.27	140	1.03 *	0.27	3	2.63
1e						1.0 **	0.26		3
1f						1.2 **	0.31		1.45

Note: All cases correspond to a slope angle $\alpha = 40^\circ$ and $B^* = B = 0.75$.

* Ratio computed with equation (71), assuming $A = A^*$.

** Ratio assumed based on expected decrease/increase of shear strength.

Results

Case	FS [-]	x_c [-]	y_c [-]	$x_1; x_2$ [-]	$y_1; y_2$ [-]	x_3 [-]	y_3 [-]
1	1.75	-24.91	130.22	0.00	0.00	93.93	71.16
1a	1.57	-24.91	130.22	0.00	0.00	93.93	71.16
1b	1.75						
1c	1.22						
1d	1.81	-24.91	130.22	0.00	0.00	93.93	71.16
1e	1.75						
1f	2.10						

factors of safety for Cases 1c and 1f result even smaller and larger, respectively, than that for Case 1 (i.e., $1.22 < 1.75 < 2.10$).

The Indraratna et al. constitutive model was written in the internal scripting language of the software FLAC (Itasca Consulting Group, Inc. 2016) and the rockfill slope stability problem for all cases included in Tables 8 and 9 were solved using the parametric mesh of elements in Figure 24a. The FLAC models implemented the *shear strength reduction technique* (see, for example, Griffiths & Lane 1999) to define the values of factor of safety and outline the contours of shear strain at the verge of failure. Figure 24b shows the shear strength reduction technique results for the Cases 1, 2, 4 and 5 in Table 8 (other computed cases look similar and are not included here for space reasons). The factors of safety obtained with FLAC are listed in the legend. These values compare reasonably well with those obtained with the limit equilibrium software SLIDE. Superimposed to the contours of shear strain, the plots in Figure 24b include the outline of the critical circular failure surface obtained with SLIDE. The position of the critical failure surfaces obtained with the two methods are slightly different, due to the fact that actual critical failure surfaces are not a perfect arcs of circles, as considered in the SLIDE models —see Carranza-Torres (2021).

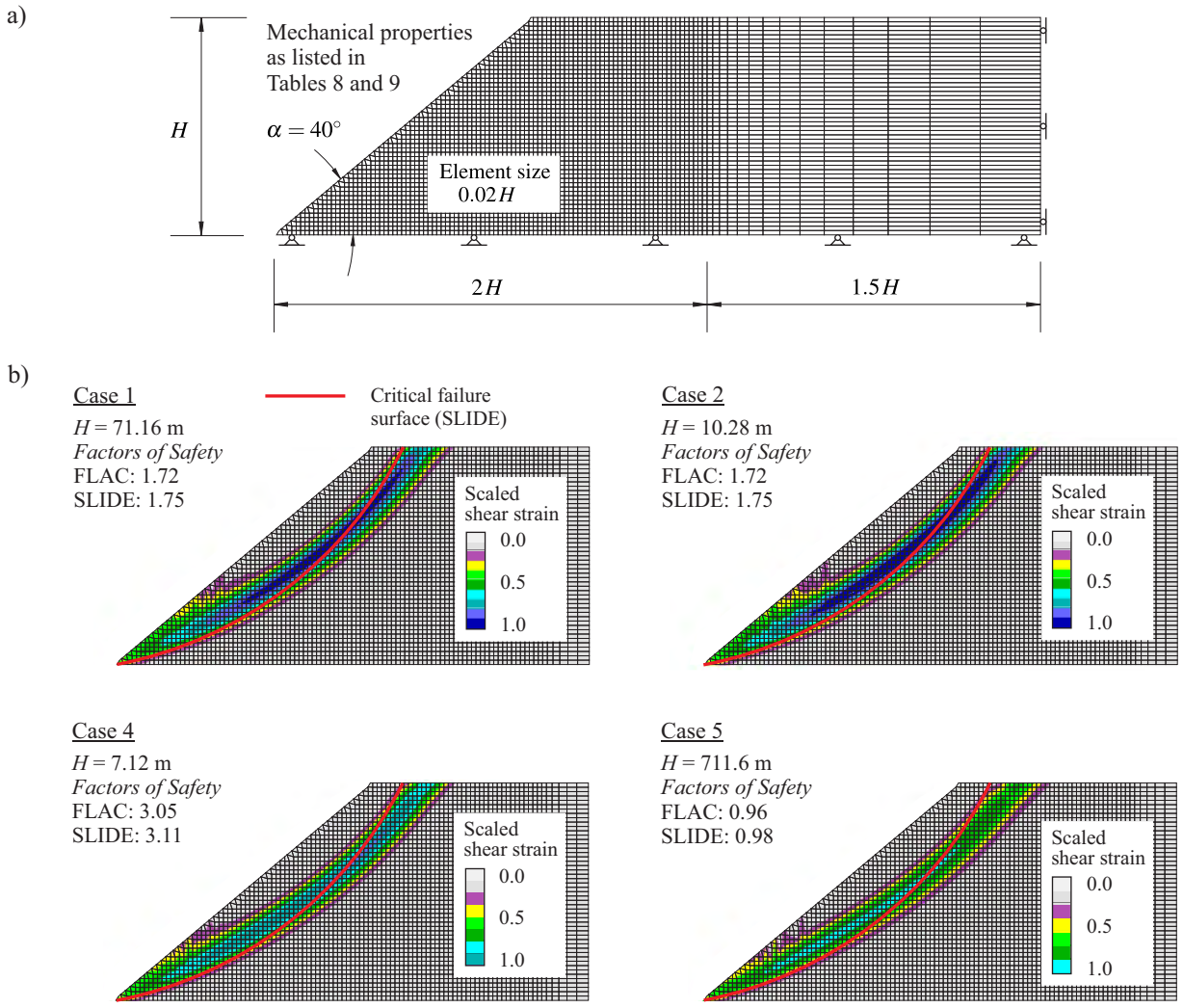

Figure 24. a) FLAC mesh used to model various rockfill slope cases. b) Critical failure surfaces for various cases in Table 8, obtained with the software FLAC and SLIDE.

7. CONCLUSIONS

This paper has presented the formulation of a general power law failure criterion for intact rock, expressed in terms of principal stresses and in terms of stresses on the failure plane, that has the Mohr-Coulomb, Hoek-Brown and Fairhurst failure criteria as particular cases of the general failure criterion. It has presented also the formulation of a general power law failure criterion for cemented and uncemented rockfill interfaces, expressed in terms of stresses on the failure plane, that has the model by Indraratna et al. for uncemented rockfill as particular case of the general failure criterion.

The paper has provided the set of equations needed to transform the general power law failure criterion expressed in terms of principal stresses to the equivalent failure criterion expressed in terms of stresses on the failure plane, and vice-versa. This set of equations are hoped to contribute to the needed implementation of power law models in finite difference and finite element rock engineering software, particularly for modelling cemented and uncemented rockfill material.

The paper has outlined a general rule to scale the proposed power law failure criterion and consequently to scale all shear failure criteria mentioned earlier. The use of the scaled form of the failure criteria has been illustrated with the analysis and interpretation of actual shear strength test results for intact rock and uncemented rockill.

As a practical application of the scaling rule for intact rock, the paper has discussed the generalization in the interpretation of the damage around sections of circular holes based on elasto-plastic analytical and semi-analytical solutions for the Mohr-Coulomb, Hoek-Brown and Fairhurst failure criteria. So called *global* ground reaction curves that summarize all possible ground reaction curves that can be obtained for these failure criteria have been introduced.

Although the elasto-plastic solution of a circular hole subjected to uniform initial stresses in homogeneous and isotropic rock that obeys the Mohr-Coulomb and Hoek-Brown failure criteria has been presented in many publications in the past, to the author's knowledge, the solution for the case of a rock that obeys the Fairhurst failure criterion, and consequently the Griffith failure criterion, has not been published before. The semi-analytical solution for Fairhurst failure criterion may be of practical application to quantity the extent of fracturing damage around holes.

Finally, and as a practical application of the scaling law for rockfill, the paper has presented the generalization in the interpretation of the factor of safety and location of the critical failure surface for slopes in uncemented rockfill slopes that satisfy the Indraratna et al. failure criterion.

REFERENCES

Baker, R. 2004. Nonlinear Mohr envelopes based on triaxial data. *Journal of Geotechnical and Geoenvironmental Engineering 130*(5), 498–506.

Balmer, G. 1952. A general analytical solution for Mohr's envelope. *Proceedings of American Society of Test Materials* (52), 1260–1271.

Carranza-Torres, C. 1998. *Self-similarity analysis of the elasto-plastic response of underground openings in rock and effects of practical variables*. Phd thesis, University of Minnesota.

Carranza-Torres, C. 2002. Dimensionless charts for the evaluation of the elasto-plastic response of tunnels in rock. In *Proceedings of NARMS-TAC 2002, Mining Innovation and Technology. Toronto. July 10, 2002*, pp. 1133–1143. University of Toronto.

Carranza-Torres, C. 2003. Dimensionless graphical representation of the exact elasto-plastic solution of a circular tunnel in a Mohr-Coulomb material subject to uniform far-field stresses. *Rock Mechanics and Rock Engineering 36*(3),

237–253.

Carranza-Torres, C. 2021. Computational tools for the analysis of circular failure of rock slopes. Keynote Lecture. In *Proceedings of EUROCK 2021. Mechanics and Rock Engineering from Theory to Ppractice. Turin, Italy. September 21–24, 2021*. Pre-print available for downloading at www.d.umn.edu/∼carranza/EUROCK21.

Carranza-Torres, C. & Fairhurst, C. 1999. The elasto-plastic response of underground excavations in rock masses that satisfy the Hoek-Brown failure criterion. *International Journal of Rock Mechanics and Mining Sciences 36*(8), 777–809.

Carranza-Torres, C. & Hormazabal, E. 2018. Computational tools for the estimation of factor of safety and location of the critical failure surface for slopes in Mohr-Coulomb dry ground. In *Proceedings of the 2018 International Symposium on Slope Stability in Open Pit Mining and Civil Engineering. Sevilla, Spain, April 11–13, 2018*. Australian Centre for Geomechanics: Pre-print available for downloading at www.d.umn.edu/∼carranza/SLOPE18.

Carranza-Torres, C. & Hormazabal, E. 2020. Computational tools for the estimation of factor of safety and location of the critical failure surface for slopes in rock masses that satisfy the Hoek-Brown failure criterion. In *Proceedings of the 2020 International Symposium on Slope Stability in Open Pit Mining and Civil Engineering. Perth, Australia, May 12–14, 2020*, pp. 1099–1122. Australian Centre for Geomechanics: Pre-print available for downloading at www.d.umn.edu/∼carranza/SLOPE20.

Davis, R. O. & Selvadurai, A. P. S. 1996. *Elasticity and geomechanics*. Cambridge University press.

Davis, R. O. & Selvadurai, A. P. S. 2002. *Plasticity and geomechanics*. Cambridge University press.

de Mello, F. B. 1977. Reflections on design decisions of practical significance to embankment dams. *Géotechnique 27*(3), 281–355.

Detournay, E. 1986. Elastoplastic model of a deep tunnel for a rock with variable dilatancy. *Rock Mechanics and Rock Engineering 19*(2), 99–108.

Fairhurst, C. 1964. On the validity of the 'Brazilian' test for brittle materials. *International Journal of Rock Mechanics and Mining Sciences & Geomechanics Abstracts 1*(4), 535–546.

Goodman, R. E. 1989. *Introduction to rock mechanics* (Second ed.). Wiley.

Griffith, A. A. 1921. The phenomena of rupture and flow in solids. *Philosophical Transactions of the Royal Society A: Mathematical, Physical and Engineering Sciences 221*(582-593), 163–198.

Griffith, A. A. 1924. Theory of rupture. In *Proc. 1st. Int. Cong. Appl. Mech., Delft*, pp. 55–63.

Griffiths, D. V. & Lane, P. A. 1999. Slope stability analysis by finite elements. *Géotechnique 49*(3), 387–403.

Hoek, E. 1965. *Rock fracture under static stress conditions*. Phd thesis, University of Cape Town.

Hoek, E. & Bieniawski, Z. T. 1966. Facture propagation mechanism in hard rock. In *Proc. 1st. Congr. Int. Soc. Rock Mech.*, 1, Lisbon, pp. 243–249.

Hoek, E. & Bray, J. 1981. *Rock Slope Engineering*. Spon Press.

Hoek, E. & Brown, E. T. 1980a. Empirical strength criterion for rock masses. *J. Geotech. Eng. Div. ASCE 106*(GT9), 1013–1035.

Hoek, E. & Brown, E. T. 1980b. *Underground Excavations in Rock*. London: The Institute of Mining and Metallurgy.

Hoek, E. & Brown, E. T. 2019. The Hoek-Brown failure criterion and GSI – 2018 edition. *Journal of Rock Mechanics and Geotechnical Engineering 11*(3), 445–463.

Hoek, E., Carranza-Torres, C. & Corkum, B. 2002. Hoek-Brown failure criterion – 2002 edition. In *Proceedings of NARMS-TAC 2002, Mining Innovation and Technology. Toronto. July 10, 2002*, pp. 267–273. University of Toronto.

Hoek, E. & Martin, C. D. 2014. Fracture initiation and propagation in intact rock – A review. *Journal of Rock Mechanics and Geotechnical Engineering 6*(4), 287–300.

Indraratna, B., Wijewardena, L. S. S. & Balasubramaniam, A. S. 1993. Large-scale triaxial testing of greywacke rockfill. *Géotechnique 43*(1), 37–51.

Itasca Consulting Group, Inc. 2016. *FLAC (Fast Lagrangian Analysis of Continua) Version 8.0*. Minneapolis, Minnesota.

Jaeger, J. C., Cook, N. G. W. & Zimmerman, R. 2007. *Fundamentals of rock mechanics* (Fourth ed.). Blackwell Publishing.

Jiang, J., Baker, R. & Yamagami, T. 2003. The effect of strength envelope nonlinearity on slope stability computations. *Canadian Geotechnical Journal 40*(2), 308–325.

Linero, S., Palma, C. & Apablaza, R. 2007. Geotechnical characterisation of waste material in very high dumps with large scale triaxial testing. In *Slope Stability 2007: Proceedings of the 2007 International Symposium on Rock Slope Stability in Open Pit Mining and Civil Engineering*, pp. 59–75. Australian Centre for Geomechanics.

Londe, P. 1988. Discussion on the determination of the shear stress failure in rock masses. *J. Geotech. Eng. Div. ASCE 114*(3), 374–376.

Marachi, N. D., Chan, C. K. & Seed, H. B. 1972. Evaluation of properties of rockfill materials. *Journal of the Soil Mechanics and Foundations Division ASCE 98*(1), 95–114.

Marsal, R. J. 1967. Large scale testing of rockfill materials. *Journal of the Soil Mechanics and Foundations Division ASCE 93*(2), 27–43.

Murrell, S. A. F. 1958. The strength of coal under triaxial compression. *Mechanical properties of non-metallic brittle materials*, 123–145.

Ovalle, C., Linero, S., Dano, C., Bard, E., Hicher, P. Y. & Osses, R. 2020. Data compilation from large drained compression triaxial tests on coarse crushable rockfill materials. *Journal of Geotechnical and Geoenvironmental Engineering 146*(9), 06020013.

Press, W. H., Teukolsky, S. A., Vetterling, W. T. & Flannery, B. P. 2007. *Numerical recipes: The art of scientific computing* (Third ed.). Cambridge University Press.

Ramsey, J. M. & Chester, F. M. 2004. Hybrid fracture and the transition from extension fracture to shear fracture. *Nature 428*(6978), 63–66.

Rocscience Inc. 2018. *SLIDE 2018. Slope stability analysis software based on the limit equilibrium method*. Toronto, Canada.

Rojat, F. 2010. *Comportement des tunnels dans les milieux rocheux de faibles caractéristiques mécaniques*. Phd thesis, Ecole des Ponts ParisTech.

Yu, H., Ng, K., Grana, D., Alvarado, V., Kaszuba, J. & Campbell, E. 2020. A generalized power-law criterion for rocks based on Mohr failure theory. *International Journal of Rock Mechanics and Mining Sciences 128*(104274), 1–8.

APPENDIX A. POWER LAW FAILURE CRITERIA EXPRESSED IN TERMS OF PRINCIPAL STRESSES AND STRESSES ON THE FAILURE PLANE

In Section 2.1, equations (10) and (11) are the generic form of the set of equations needed to transform the general power law failure criterion given by equation (8), into an equivalent failure criterion expressed in terms of normal and shear stresses on the failure plane. To simplify notation, in this appendix a tilde above a stress variable is used to indicate that the stress has been divided by the unconfined compression strength, σ_c.

The explicit form of equations (10) and (11) are the equations due to Balmer (1952). These are

$$\tilde{\sigma}_n = \frac{\tilde{\sigma}_1 + \tilde{\sigma}_3}{2} - \frac{\tilde{\sigma}_1 - \tilde{\sigma}_3}{2} \frac{\mathrm{d}\tilde{\sigma}_1/\mathrm{d}\tilde{\sigma}_3 - 1}{\mathrm{d}\tilde{\sigma}_1/\mathrm{d}\tilde{\sigma}_3 + 1} \tag{A-1}$$

and

$$\tilde{\tau}_s = (\tilde{\sigma}_1 - \tilde{\sigma}_3) \frac{\mathrm{d}\tilde{\sigma}_1/\mathrm{d}\tilde{\sigma}_3 - 1}{\mathrm{d}\tilde{\sigma}_1/\mathrm{d}\tilde{\sigma}_3 + 1} \tag{A-2}$$

For the general power law failure criterion given by equation (8), the derivatives in equations (A-1) and (A-2)

are

$$\frac{\mathrm{d}\tilde{\sigma}_1}{\mathrm{d}\tilde{\sigma}_3} = 1 + CD\left(\tilde{\sigma}_3 - \tilde{\sigma}_{tBx}\right)^{D-1} \tag{A-3}$$

In Section 2.1, equations (13) and (14) are the generic form of the set of equations needed to transform the general power law failure criterion given by equation (12), into an equivalent failure criterion expressed in terms of principal stresses. Application of the inverse of the equations (A-1) and (A-3) allows, in principle, the relationships in equations (13) and (14) to be obtained, but since the procedure requires use of numerical methods of integration, explicit (closed-form) equations are not be possible.

An alternative procedure for recasting the general power law failure criterion expressed in terms of shear and normal stresses on the failure plane, into an equivalent failure criterion expressed in terms of principal stresses, is to express the power law failure criterion directly in terms of principal stresses. For the case $0.5 \leq B < 1$, the equivalent failure criterion takes the following form

$$\left(\frac{\tilde{\sigma}_1 - \tilde{\sigma}_3}{2}\right)^2 \left[1 - \left[\frac{\tilde{\sigma}_1 + \tilde{\sigma}_3 - 2\tilde{\sigma}_{tBx}}{2(1-B)(\tilde{\sigma}_1 - \tilde{\sigma}_3)} - \sqrt{\left[\frac{\tilde{\sigma}_1 + \tilde{\sigma}_3 - 2\tilde{\sigma}_{tBx}}{2(1-B)(\tilde{\sigma}_1 - \tilde{\sigma}_3)}\right]^2 - \frac{B}{1-B}}\right]^2\right] \tag{A-4}$$

$$-A^2\left[\frac{\tilde{\sigma}_1 + \tilde{\sigma}_3}{2} - \frac{\tilde{\sigma}_1 - \tilde{\sigma}_3}{2}\left[\frac{\tilde{\sigma}_1 + \tilde{\sigma}_3 - 2\tilde{\sigma}_{tBx}}{2(1-B)(\tilde{\sigma}_1 - \tilde{\sigma}_3)} - \sqrt{\left[\frac{\tilde{\sigma}_1 + \tilde{\sigma}_3 - 2\tilde{\sigma}_{tBx}}{2(1-B)(\tilde{\sigma}_1 - \tilde{\sigma}_3)}\right]^2 - \frac{B}{1-B}}\right] - \tilde{\sigma}_{tBx}\right]^{2B} = 0$$

Details of the procedure for obtaining an equivalent version of equation (A-4) are outlined in Yu et al. (2020).

APPENDIX B. SCALING OF THE GENERALIZED HOEK-BROWN FAILURE CRITERION

The generalized Hoek-Brown failure criterion for rock masses is written as follows —see for example, Hoek & Brown (1980a; 1980b)

$$\frac{\sigma_1}{\sigma_c} = \frac{\sigma_3}{\sigma_c} + \left(m_b \frac{\sigma_3}{\sigma_c} + s\right)^a \tag{B-1}$$

where σ_c is the unconfined compression strength of the intact rock and m_b, s and a are parameters of the rock mass. These parameters depend on the parameter m_i for intact rock (discussed in the main text), on the Geological Strength Index, *GSI*, and on the Disturbance Factor, D (Hoek et al. 2002; Hoek & Brown 2019).

Considering that the biaxial tensile strength of the rock mass, σ_{tBx}, corresponds to the case, $\sigma_1 = \sigma_3$ in equation (B-1), then

$$\frac{\sigma_{tBx}}{\sigma_c} = -\frac{s}{m_b} \tag{B-2}$$

Replacing equation (B-2) into equation (B-1), and factoring terms, the generalized Hoek-Brown failure criterion can be written as follows

$$\frac{\sigma_1}{\sigma_c} = \frac{\sigma_3}{\sigma_c} + {m_b}^a \left(\frac{\sigma_3}{\sigma_c} - \frac{\sigma_{tBx}}{\sigma_c}\right)^a \tag{B-3}$$

Comparing the equation (B-2) with equation (8), the generalized Hoek-Brown failure criterion is found to be

a particular case of the general power law failure criterion given by equation (8), when

$$C = {m_b}^a \qquad D = a \quad \text{and} \quad E = 0 \tag{B-4}$$

Replacing equations (B-4) into equation (49), the scaled form of the generalized Hoek-Brown failure criterion results to be

$$S_1 = S_3 + S_3^a \tag{B-5}$$

where

$$S_1 = \left(\frac{\sigma_1}{\sigma_c} + \frac{s}{m_b}\right) m_b^{-a/(1-a)} \quad \text{and} \quad S_3 = \left(\frac{\sigma_3}{\sigma_c} + \frac{s}{m_b}\right) m_b^{-a/(1-a)} \tag{B-6}$$

Equations (B-5) and (B-6) correspond to the scaled version of the Hoek-Brown failure criterion for rock masses proposed by Rojat (2010).

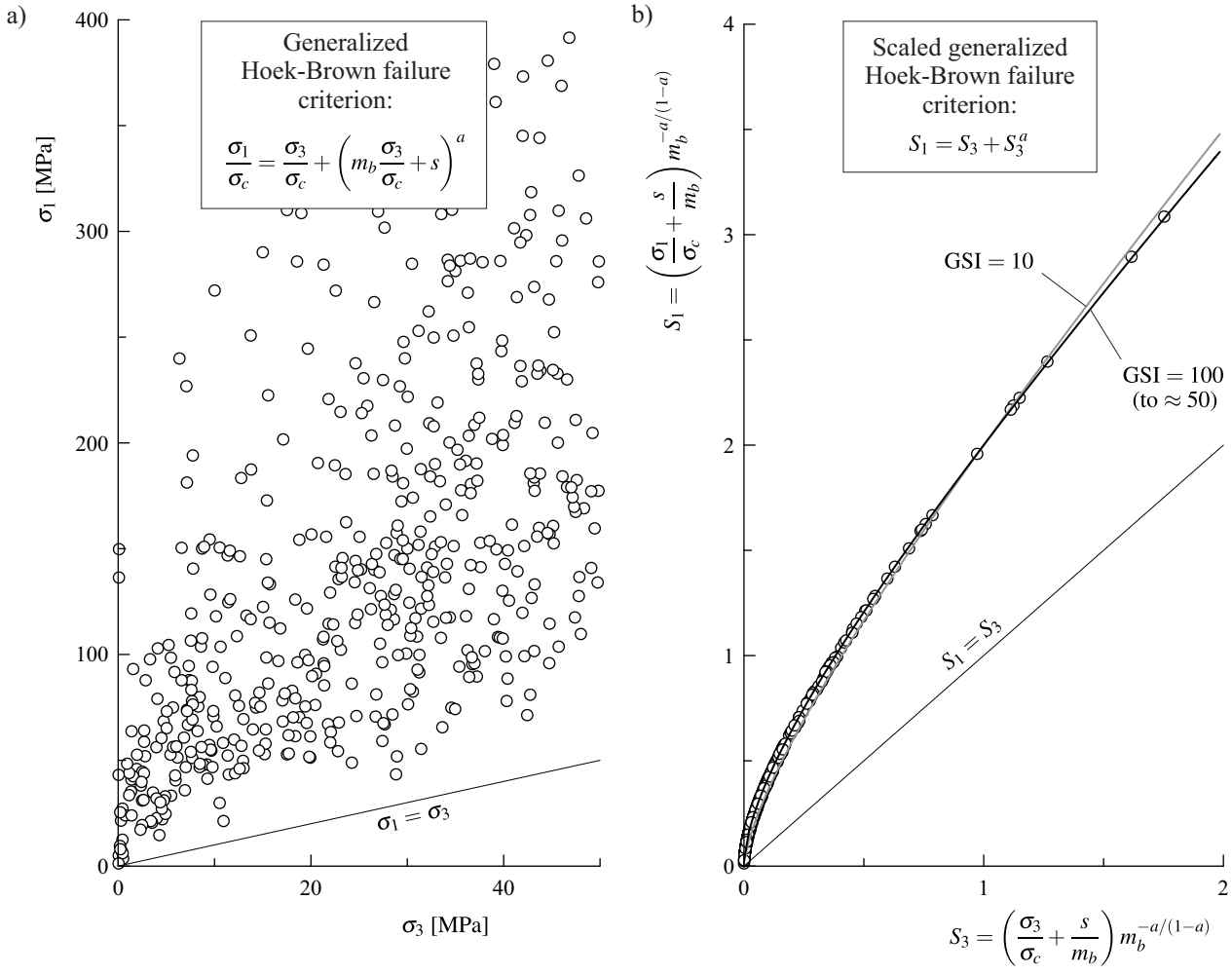

Figure B.1. Major principal stresses at failure according to the generalized Hoek-Brown failure criterion for 1,000 randomly generated cases (from a uniform distribution) of confining stresses. Representation in terms of a) actual stresses, and b) scaled stresses according to equations (B-6).

APPENDIX C. SELF-SIMILAR ANALYSIS OF THE MECHANICAL RESPONSE OF A CIRCULAR HOLE IN A ROCK THAT OBEYS THE POWER LAW FAILURE CRITERION

This appendix presents the plane-strain elasto-plastic formulation of the problem of driving a circular borehole in a homogeneous isotropic perfectly plastic medium, initially subjected to uniform (hydrostatic) compressive stresses (see Figure 12a). The formulation is based on the incremental theory of plasticity, and takes advantage of the self-similar nature of the problem, discussed in Detournay (1986).

The formulation that follows assumes that the internal pressure in the hole has fallen below the critical pressure, p_i^{cr}, and that the plastic region of radial extent R_{pl} develops.

The yield function of the material is defined by an arbitrary function 'Y' of the scaled principal stresses, S_1 and S_3, i.e.,

$$Y(S_1, S_3) = 0 \tag{C-1}$$

In equation (C-1), and in all equations in this appendix, capital 'S' refers to principal stresses that have been scaled according to the scaling rule introduced in Section 3.1.

The flow rule of the material is assumed to be non-associated, with a linear potential function of scaled principal stresses as follows

$$F(S_1, S_3) = S_1 - K_\psi S_3 = 0 \tag{C-2}$$

In equation (C-2), K_ψ is computed based on the plastic dilation angle, ψ, as in equation (89).

For the hole *excavation* problem in Figure 12a, for which the internal pressure decreases below the far-field stress, the hoop stresses are major principal stresses and the radial stresses are minor principal stresses, i.e.,

$$S_1 = S_\theta \qquad \text{and} \qquad S_3 = S_r \tag{C-3}$$

According to Detournay (1986), the extent of the plastic region, R_{pl}, is a kinematic parameter that can be used to integrate the incremental equations of elasto-plasticity. Consequently, the dimensionless variable, ρ, is defined to be a function of the radial distance, r, and the variable R_{pl} as follows

$$\rho = \frac{r}{R_{pl}} \tag{C-4}$$

Equation (C-4) maps the physical plane of coordinate r into a 'unit circle' of radius equal to one, where the boundary of the unit circle represents the boundary of the plastic region in the physical plane.

Figure 12a shows the radial displacement $u(r)$ for a point at the radial distance r from the center. In the formulation below, capital 'U' will be used to indicate that the radial displacement is now a function of the scaled radial distance, ρ, defined by equation (C-4) —i.e., $U(\rho)$ refers to the radial displacement in the unit circle. In addition, a tilde above the capital 'U' will indicate that the radial displacement has been scaled as follows

$$\tilde{U}_r(\rho) = 2\tilde{G}\,\frac{U_r(\rho)}{R} \tag{C-5}$$

where

$$\tilde{G} = \frac{G}{\sigma_c}\,C^{-1/(1-D)} \qquad \text{if} \qquad 0.5 \le D < 1 \tag{C-6}$$

and

$$\tilde{G} = \frac{G}{\sigma_c} \qquad \text{if} \qquad D = 1 \tag{C-7}$$

In equations (C-6) and (C-7), G is the elastic shear modulus of the material.

As discussed in Section 2.2, for the case of Mohr-Coulomb material, $D = 1$; therefore, the scaled shear modulus for this case is given by equation (C-7).

As dicussed in Section 2.3, for the case of Hoek-Brown rock, $C = \sqrt{mi}$ and $D = 1/2$; therefore, replacing these values in equation (C-6), the scaled shear modulus for Hoek-Brown rock becomes

$$\tilde{G} = \frac{G}{\sigma_c} \frac{1}{m_i} \tag{C-8}$$

Similarly, and as discussed in Section 2.4, for the case of Fairhurst rock $C = 2(\sqrt{n_i + 1} - 1)/\sqrt{n_i}$ and $D = 1/2$; therefore, replacing these values in equation (C-6), the scaled shear modulus for Fairhurst rock becomes

$$\tilde{G} = \frac{G}{\sigma_c} \frac{n_i}{4\left(\sqrt{n_i + 1} - 1\right)^2} \tag{C-9}$$

Due to the self-similar nature of the problem, the relationship between the radial displacement $u(r)$ in the physical plane and the radial displacement $U(\rho)$ in the unit circle must be —see Detournay (1986)

$$u_r(r) = \frac{R_{pl}}{2\tilde{G}} \tilde{U}_r(\rho) \tag{C-10}$$

The differential equations governing the hole excavation problem are as follows —see Carranza-Torres (1998; 2002)

$$\frac{\mathrm{d}S_r}{\mathrm{d}\rho} = -\frac{S_r - S_\theta}{\rho} \tag{C-11}$$

$$\frac{\mathrm{d}S_\theta}{\mathrm{d}\rho} = -\frac{1}{B_2}\left[B_1 \frac{\mathrm{d}S_r}{\mathrm{d}\rho} - B_3 \rho \frac{\mathrm{d}^2\tilde{U}_r}{\mathrm{d}\rho^2} + B_4\right] \tag{C-12}$$

$$\frac{\mathrm{d}^2\tilde{U}_r}{\mathrm{d}\rho^2} = A_2 \frac{\mathrm{d}S_r}{\mathrm{d}\rho} - A_3 \frac{\mathrm{d}S_\theta}{\mathrm{d}\rho} + \frac{A_1}{\rho} \frac{\mathrm{d}\tilde{U}_r}{\mathrm{d}\rho} - A_1 \frac{\tilde{U}_r}{\rho^2} \tag{C-13}$$

where

$$A_1 = \frac{\partial F/\partial S_r}{\partial F/\partial S_\theta} = -K_\psi \tag{C-14}$$

$$A_2 = 1 - \nu + \nu \frac{\partial F/\partial S_r}{\partial F/\partial S_\theta} = 1 - \nu - K_\psi \nu \tag{C-15}$$

$$A_3 = (1 - \nu) \frac{\partial F/\partial S_r}{\partial F/\partial S_\theta} + \nu = \nu - K_\psi (1 - \nu) \tag{C-16}$$

and

$$B_1 = \partial Y/\partial S_r \tag{C-17}$$

$$B_2 = \partial Y/\partial S_\theta \tag{C-18}$$

$$B_3 = 0 \tag{C-19}$$

$$B_4 = 0 \tag{C-20}$$

Equation (C-11) represents equilibrium, equation (C-12) represents the consistency condition, and equation (C-13) represents compatibility of deformation.

Four boundary conditions are needed to integrate the set of differential equations (C-11) through (C-13) (Carranza-Torres 1998; 2002).

The first boundary condition is

$$S_r(1) = P_i^{cr} \tag{C-21}$$

where P_i^{cr} is scaled critical internal pressure below which the plastic region develops. This is computed from the solution of the following system of equations

$$Y(S_1, P_i^{cr}) = 0 \tag{C-22}$$

$$S_1 - 2S_o + P_i^{cr} = 0 \tag{C-23}$$

The second boundary condition is the value $S_\theta(1)$, that can be found from the yield function in equation (C-1)

$$Y(S_\theta(1), P_i^{cr}) = 0 \tag{C-24}$$

The third boundary condition is the value $\tilde{U}_r(1)$, that is computed from the elastic solution of the region surrounding the plastic region, i.e.,

$$\tilde{U}_r(1) = S_o - P_i^{cr} \tag{C-25}$$

Finally, the fourth third boundary condition is

$$\frac{\mathrm{d}\tilde{U}_r(1)}{\mathrm{d}\rho} = -(S_o - P_i^{cr}) \tag{C-26}$$

Equation (C-26) has been obtained by differentiation of equation (C-10), together with equation (C-25).

Once the scaled radial stress function $S_r(\rho)$ and the hoop stress function $S_\theta(\rho)$ have been obtained, the extent of plastic failure, R_{pl}, can be found from the condition that at the wall of the hole (i.e., at $\rho = R/R_{pl}$), $S_r(\rho)$ must be equal to the scaled internal pressure, P_i.